AD-A188 683 SUB-SCALING OF PROJECTILE/TARGET SYSTEM DAMAGED BY HYPERVELOCITY(U) COMPTEK CORP ALLENTOWN PA G C SIH MAR 87 MTL-TR-87-17 DAAG46-85-C-0061 1/1

UNCLASSIFIED F/G 19/10 NL

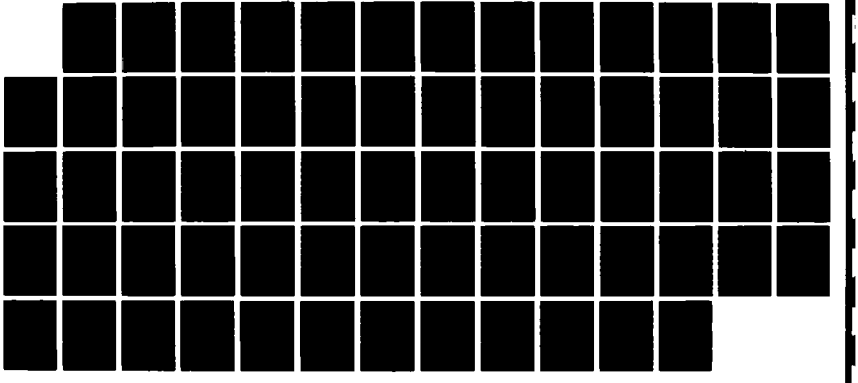

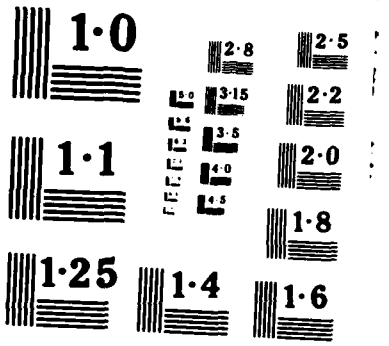
1·0
1·1
1·25
1·4
1·6
1·8
2·0
2·2
2·5
2·8
3·15
3·5
4·0
4·5
5·0
5·6
6·3
7·1
8·0
9·0
10·0

AD

MATERIALS TECHNOLOGY
LABORATORY

MTL TR 87-17

SUB-SCALING OF PROJECTILE/TARGET SYSTEM DAMAGED BY HYPERVELOCITY

March 1987

G. C. SIH
Comptek Corporation
Allentown, PA 18103

FINAL REPORT

Contract No. DAAG46-85-C-0061

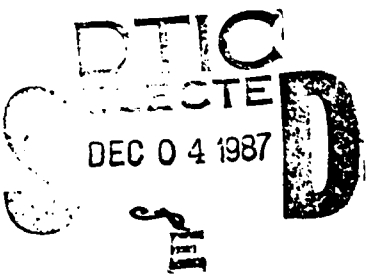

Prepared for

U.S. ARMY MATERIALS TECHNOLOGY LABORATORY
Watertown, Massachusetts 02172-0001

REPORT DOCUMENTATION PAGE

READ INSTRUCTIONS BEFORE COMPLETING FORM

1. REPORT NUMBER: MTL TR 87-17	2. GOVT ACCESSION NO.
3. RECIPIENT'S CATALOG NUMBER	
4. TITLE (and Subtitle): SUB-SCALING OF PROJECTILE/TARGET SYSTEM DAMAGED BY HYPERVELOCITY	5. TYPE OF REPORT & PERIOD COVERED: Final Report 8/28/85 through 9/30/86
	6. PERFORMING ORG. REPORT NUMBER
7. AUTHOR(s): G. C. Sih	8. CONTRACT OR GRANT NUMBER(s): DAAG46-85-C-0061
9. PERFORMING ORGANIZATION NAME AND ADDRESS: Comptek Corporation, 2400 Schoenersville Road, RD 4, Allentown, PA 18103	10. PROGRAM ELEMENT, PROJECT, TASK AREA & WORK UNIT NUMBERS: AMCMS Code: 69200R.897 A050
11. CONTROLLING OFFICE NAME AND ADDRESS: U.S. Army Materials Technology Laboratory, ATTN: SLCMT-ISC, Watertown, MA 02172-0001	12. REPORT DATE: March 1987
	13. NUMBER OF PAGES: 54
14. MONITORING AGENCY NAME & ADDRESS (if different from Controlling Office)	15. SECURITY CLASS. (of this report): Unclassified
	15a. DECLASSIFICATION/DOWNGRADING SCHEDULE

16. DISTRIBUTION STATEMENT (of this Report)

Approved for public release; distribution unlimited.

17. DISTRIBUTION STATEMENT (of the abstract entered in Block 20, if different from Report)

18. SUPPLEMENTARY NOTES

19. KEY WORDS (Continue on reverse side if necessary and identify by block number)

Hypervelocity impact
Scale models
Damage
Fracture
Finite element
Strain energy methods
Numerical analysis
Phase transformation

20. ABSTRACT (Continue on reverse side if necessary and identify by block number)

(SEE REVERSE SIDE)

DD FORM 1 JAN 73 1473 EDITION OF 1 NOV 65 IS OBSOLETE

Block No. 20

ABSTRACT

Preliminary efforts are made to develop a methodology for analyzing the progressive failure of projectile/target systems under hypervelocity impact. Particular emphasis is placed on the thermal/mechanical interaction effects not only for evaluating the change in the local strain rates and material properties but also in finding the temperature and latent heat at which the solid may locally transform into liquid and/or gas. Such a transition can be accurately determined by the inflection points on the time dependent H-function curve that serves as a measure of the order and/or disorder of a physical system.

Damage of a tungsten projectile with a 1:3.57 aspect ratio impacting a 5083 aluminum target with a 1:3 aspect ratio at 9,000 m/sec is evaluated. Melting of the target material is predicted in the region directly underneath the projectile corner. Geometrically and metallurgically similar systems scaled down one-half and one-quarter in size are also considered resulting in damage zones that are not proportional. Such information is useful for developing scaling relations even though the results are nonlinear functions of the governing parameters.

TABLE OF CONTENTS

FORWARD

This investigation on hypervelocity impact has been conducted by the Comptek Corporation for the Army Materials Technology Laboratories in Watertown, Massachussetts under Contract DAAG46-85-C-0061.

The principal investigator for the study was Dr. George C. Sih who has successfully developed the basic thermodynamics for analyzing material transformation under high speed impact. Analyzed in this report is the melting of 5083 aluminum target by a tungsten projectile. Initial impact results are also obtained for projectile/target systems in full scale, half scale and quarter scale with the objective of developing sub-scaling relations.

Dr. S. C. Chou has been the AMTL technical monitor. The author wishes to thank him for providing some of the pertinent information. The encouragement and interest expressed by Mr. John F. Dignam during the course of this project are also gratefully acknowledged.

I. INTRODUCTION

When a solid comes in contact with another at high speed, there prevails locally an extremely high rate of energy transfer. The initial kinetic energy of the moving body is converted to different forms depending on the impact speed, body geometry and size and material property. If the impact velocity is sufficiently high, local material transformation can take place such that the solid may melt or even vaporize in addition to damage by permanent deformation and/or fracture. Material transformation and failure behavior are not only time varying but they are also location dependent. Quantitative assessment of these processes is, to say the least, lacking. There are still some distances from a full understanding of these processes by the engineering community, particularly in the development of analytical models which describe and characterize them in a way that can be used in design. The overwhelming difficulties do not appear to be technical but rather in overcoming preconceived ideas and theories that do not lend themselves to a consistent treatment of the physical phenomena in high speed impact.

One of the weaknesses of classical physics and mechanics when used to characterize the behavior of solid, liquid and gas is that the theoretical formulation relies upon a knowledge of the constitutive relation. As a result, a hierarchy of theories has been developed, each is being applicable over a certain range of stress, strain, strain rate, temperature and material type such as elastic or plastic solid, inviscid or viscous fluid, perfect or Van der Waal gas, etc. If in a single event, material behavior includes two or more of the aforementioned types, then the adjoining of the different theories and/or solutions in itself becomes a monumental task. There is no

hope for uniqueness unless a unified theory* can be developed that can account for all material behavior without making an a priori assumption on the knowledge of the constitutive relation.

Despite the extensive research efforts made on hypervelocity impact, it is not difficult to include from past studies [4-6] that the traditional classical physics and mechanics approaches have not led to any in-depth understanding of the impact phenomenon. Recognized is the fact that a deformable solid can undergo several stages of extreme mechanical behavior when subjected to hypervelocity impact. In the vicinity of initial contact, the solid behaves very much like a fluid because of the very high elevation of local pressure. It is tempting at this stage to model the material behavior by Stokesian fluid or to use the Navier-Stokes theory of viscous flow. In so doing, however, the fluid/solid interaction and/or coupling effects are left out as the transformation of solid to fluid occurs only *locally* while the surrounding projectile/target material is still in the solid state. The inclusion of material rigidity effects calls for the application of other theories, say the Prandtl-Reuss theory of elastic-plastic flow in conjunction with the von Mises yield condition**. Additional assumption on fracture criteria may have to be made as failure of the projectile/target system in the final stages can involve crack propagation. Since the self-contained theories for materials at different

---

*Such an approach [1] has been developed in recent years and applied to explain a number of previously not understood physical phenomena in material damage. Predictions have been made for the SAFC-40R steel [2] and 6061-T6 aluminum [3] and the results agreed very well with experiments.

**Generalization of this condition to include dilatational effects would lead to inconsistency in the plasticity theory that assumes the uniaxial data to coincide with the effective stress and effective strain curve. One of the inherent shortcomings of all classical mechanics theories involving nonlinearity and/or dissipation is their inability to translate uniaxial data to multiaxial states without invoking serious physical limitations.

stages, yield conditions and fracture criteria are *unrelated*[*], their end results would be independent. Any attempts made to connect the individual solutions will involve arbitrariness and conditions that may not be consistent with physical observations. In fact, a three-phase equation of state for metals has been proposed [3] to account for material in the solid-liquid and liquid-vapor region. Use was made of thermodynamics and many assumptions that are subject to experimental verification. The work stopped short at predicting the hydrodynamic behavior of a real material and called for the incorporation of mechanical constitutive relations. To reiterate, material behavior under hypervelocity impact cannot be consistently explained by the classical piecemeal approach.

Presented in this work is a methodology that can model the extremes of material behavior in hypervelocity impact. Constitutive relations for each element in the projectile/target system are developed according to the rate of energy transmission and dissipation. All forms of energy involving heat, sound, phase transformation, etc. are included in the theory without neglecting their coupling effects. Thermodynamics and heat transfer should be an inherent[**] part of mechanical deformation. Only in this way, a complete and consistent description of the material in the solid, liquid and gaseous state can be given. This knowledge is pertinent for developing subscaling relations for the hypervelocity impact of projectile/target systems. Compared are the damage behavior

---

[*] Energy used and dissipated during phase transformation of material in solid state to the fluid state for example would not be accounted for.

[**] The reason that thermal/mechanical coupling effects have not been satisfactorily treated up to now is because thermodynamics, heat transfer and mechanical deformation are regarded as separate individual disciplines in classical physics and mechanics.

of full scale, half scale and quarter scale projectile/target systems. The variations of geometric and kinematic parameters with target damage are also discussed as the solid transforms into fluid in a local region. As the complete time history of material behavior under hypervelocity impact is made available, sub-scaling tests can then be designed to simulate the conditions of the full scale projectile/target system.

II. ENERGY DENSITY THEORY

Energy can be converted from one form to another and this process is inherently irreversible. The conversion of mechanical work to heat, for example, must necessarily involve energy dissipation that is unrecoverable. Even if the process were carried out adiabatically by insulating the system, *local* irreversibility can still prevail as the collision of molecules will involve energy loss. That is, each element within the system can be disturbed permanently. Local and/or global temperature change is the result. The a priori assumption that the different forms of energy such as heat, sound, etc. can be summed will encounter fundamental difficulties when analyzing coupling effects. Nonlinearity in its entirety cannot be approached by adding more terms.

2.1 Energy Conversion

Without loss in generality, the energy density theory [1,2] considers energy in two basic forms. The portion which has already dissipated and the remainder that is still available. Energy conversion involves only the exchange* of surface energy density $(dW/dA)_i$ $(i = \xi,\eta,\zeta)$ and volume energy

*As a special case, consider the equilibrium of a spherical liquid bubble of radius R under uniform pressure p. Equation (1) yields the well known result $pR = 2\gamma$ since $dW/dV = p$, $dV/dA = R/2$ and $dW/dA = \gamma$, the surface tension of the liquid.

density dW/dV at a given time t, i.e.,

$$\left(\frac{dW}{dA}\right)_i = \left(\frac{dV}{dA}\right)_i \frac{dW}{dV}, \quad i = \xi,\eta,\zeta \tag{1}$$

Here, ξ,η and ζ refer to the plane of homogeneity and are different from the reference axes x,y and z. On this plane, the surface energy density is assumed to be the same in all three mutually perpendicular directions for a homogeneous and isotropic solid:

$$\left(\frac{dW}{dA}\right)_\xi = \left(\frac{dW}{dA}\right)_\eta = \left(\frac{dW}{dA}\right)_\zeta = \left(\frac{dW}{dA}\right)_o \tag{2}$$

The value $(dW/dA)_o$ is referred to the uniaxial case. The condition in equation (2) as illustrated in Figure 1, of course, must be modified for materials whose internal structure may possess preferred directions. What is important is a knowledge of the relation between $(dW/dA)_i$ $(i = \xi,\eta,\zeta)$ that establishes the plane of homogeneity. The quantity dW/dV in equation (1) is a scalar being invariant under rotation of coordinate axes. It follows that

$$\left(\frac{dV}{dA}\right)_\xi = \left(\frac{dV}{dA}\right)_\eta = \left(\frac{dV}{dA}\right)_\zeta = \left(\frac{dV}{dA}\right)_o \tag{3}$$

The change of volume with surface $(dV/dA)_i$ $(i = \xi,\eta,\zeta)$ on the plane of homogeneity are also connected. Equation (3) determines the relation between (ξ,η,ζ) and (x,y,z) because the strain components in $(dV/dA)_i$ will be known from a given deformation field. Refer to [2] for details.

2.2 Strain Function

The energy density theory requires only a knowledge of dV/dA as a

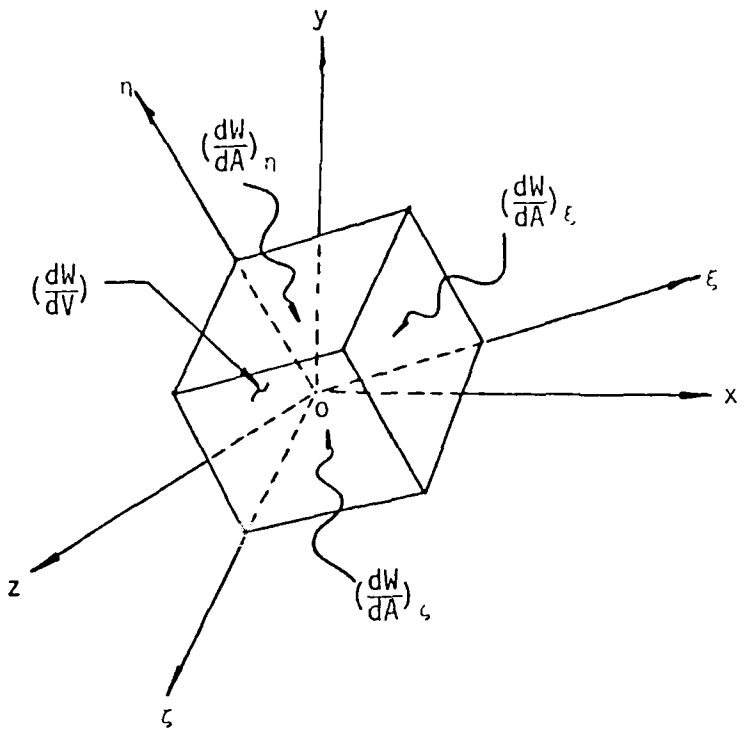

Figure 1. Plane of Homogeneity: Equal Surface Energy Density for an Isotropic and Homogeneous Body

function of uniaxial strain for the solid, liquid or gas at the initial reference state. For the fluid, strain may be expressed in terms of the ratio of volume change to volume, i.e., $\Delta V/V$. The subsequent behavior of the system is determined directly from the load-time history. The strain function

$$f(\epsilon) = \int \lambda \frac{dV}{dA} d\epsilon \qquad (4)$$

plays a fundamental role in the energy density theory from which the volume energy function in equation (1) can be obtained from a uniaxial strain state

$$\frac{dW}{dV} = \int f(\varepsilon)d\varepsilon \tag{5}$$

The parameter λ can be adjusted such that $f(\varepsilon)$ may be identified with the uniaxial stress $\sigma(\varepsilon)$. This, however, is not a necessary requirement in the energy density theory. In the case of multiaxial strain, equations (4) and (5) may be referred to the plane of homogeneity and combined to yield

$$\frac{dW}{dV} = \int\int \lambda\left(\frac{dV}{dA}\right)_i d\varepsilon_i d\varepsilon_i \quad (i = \varepsilon,\eta \text{ or } \zeta \text{ with no sum on } i) \tag{6}$$

Because of equation (3), it suffices to compute dW/dV for $i=\xi$ as follows:

$$\frac{dW}{dV} = \int\int \lambda\left(\frac{dV}{dA}\right)_\xi d\varepsilon_\xi d\varepsilon_\xi \tag{7}$$

To be emphasized is that even though equation (7) contains only the normal strain ε_ξ, dW/dV is computed for an element in a multiaxial strain state involving the influence of all the strain components via $(dV/dA)_\xi$. This provides an unique means of identifying uniaxial and multiaxial data without simplifying the physics of the problem*.

The strain function defined in equation (4) corresponds to an uniaxial strain state. In general, it may depend on the strain components ε_ξ, ε_η, etc. For an isotropic and homogeneous solid in two dimensions, the strain function may be given by

---

*The classical theory of plasticity assumes that the uniaxial data coincide with the effective stress and effective strain curve. The dilatational effects are thus neglected and cannot be accounted for by adding them into the yield condition as it would lead to inconsistency in the formulation.

$$\begin{bmatrix} f_\xi \\ f_\eta \\ f_{\xi\eta} \end{bmatrix} = \begin{bmatrix} F & & \\ & F & \\ & & G \end{bmatrix} \begin{bmatrix} \varepsilon_\xi \\ \varepsilon_\eta \\ \varepsilon_{\xi\eta} \end{bmatrix} \tag{8}$$

The functions

$$F = F[(dV/dA)_\xi, \varepsilon_\xi], \quad G = G[(dV/dA)_\xi, \varepsilon_\xi] \tag{9}$$

can be determined from the equations of motion.

2.3 Thermal/Mechanical Interaction

Classical thermodynamics associates irreversibility with entropy and heat dissipation. Since energy dissipation may take place in so many different forms, it is not justified to assume, in general, that dissipation is associated exclusively with heat loss. Referring to Figure 2, the area under opq is dW/dV or W and is divided into

$$\mathcal{D} = \left(\frac{dW}{dV}\right)_p , \quad A = \left(\frac{dW}{dV}\right)^* , \quad \mathcal{D} \geq 0 \tag{10}$$

such that $\mathcal{D}$ corresponds to opp' and A to pqp'. The corresponding strains are

$$\varepsilon = \varepsilon_p + \varepsilon^* \tag{11}$$

the dissipation energy density $\mathcal{D}$ must be a positive definite† function.

†This condition can be used as a guideline for selecting the appropriate grid size and time increment in numerical analysis.

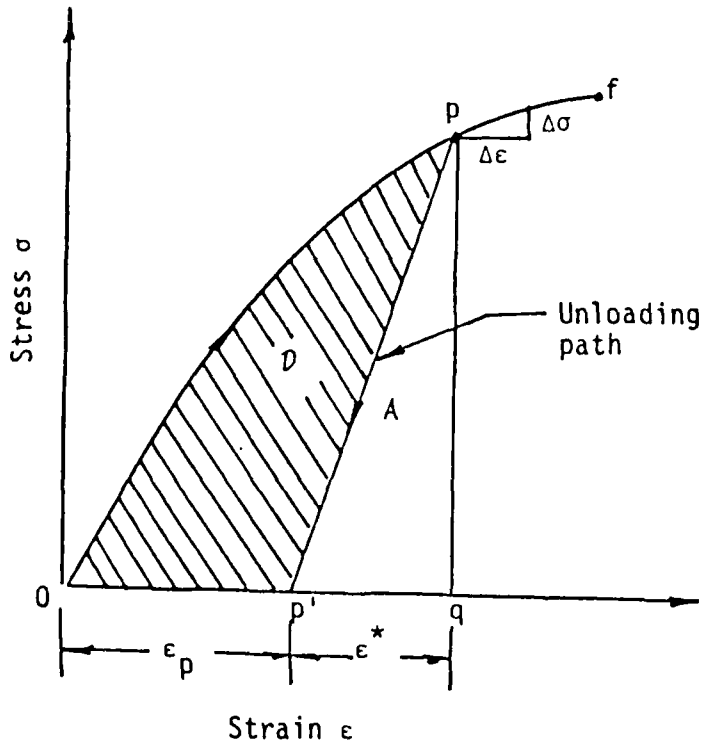

Figure 2. Uniaxial Stress and Strain Response

Because of conservation of energy, it follows that

$$dW = dD + dA, \qquad \frac{dD}{dt} \geq 0 \tag{12}$$

The rate of change of D with time is required to be a monotonically increasing function of time.

Now, let A depend on the function H and uniaxial strain* ε such that

$$A = A(H, \varepsilon) \tag{13}$$

*For a multiaxial strain state, ε_ξ on the plane of homogeneity may be used instead of ε.

Applying the rules of differentiation, equation (13) gives

$$dA = \left(\frac{\partial A}{\partial H}\right)_{\varepsilon} dH + \left(\frac{\partial A}{\partial \varepsilon}\right)_{H} d\varepsilon \tag{14}$$

Defining

$$\upsilon = \left(\frac{\partial A}{\partial H}\right)_{\varepsilon}, \qquad \sigma = \left(\frac{\partial A}{\partial \varepsilon}\right)_{H} \tag{15}$$

and differentiating equation (15), it is found that

$$\left(\frac{\partial \Theta}{\partial \varepsilon}\right)_{H} = \left(\frac{\partial \sigma}{\partial H}\right)_{\varepsilon} \tag{16}$$

With the aid of equations (12), (14) and (15), a definition of the H function is obtained:

$$-dH = \frac{d\mathcal{D}}{\Theta} \tag{17}$$

The negative sign arises as work is assumed to be done on the system rather than as done by the system in classical thermodynamics. Equation (17) resembles the classical definition of entropy as related to heat Q and temperature T. The quantity Θ may be scaled in °K as in the case of T and it becomes T only when energy dissipation occurs all in the form of heat, i.e., $\mathcal{D}$ = Q. For a finite increment of strain $\Delta\varepsilon$, it can be shown from equations (16) and (17) that

$$\frac{\Delta\Theta}{\Theta} = -\frac{\Delta\upsilon\Delta\varepsilon}{\Delta\mathcal{D}} \tag{18}$$

For an element in a multiaxial stress or strain state, equation (18) should be referred to the plane of homogeneity so that

$$\frac{\Delta\Theta}{\Theta} = -\frac{\Delta\sigma_\xi \Delta\varepsilon_\xi}{\Delta\mathcal{D}} \tag{19}$$

The temperature change at every point in the system can thus be found without invoking the separate discipline of heat transfer*. Equation (19) reveals the time nature of thermal/mechanical coupling that inherently involves energy dissipation.

2.4 Phase Change

If the rate of energy transfer in a unit volume of material becomes sufficiently intense, phase transitions in the form of melting, vaporization and sublimation can take place. The transition is strain rate dependent, an effect that is not considered explicitly in classical thermodynamics. Since transition would alter the order and disorder of the system, it would appear as an inflection point on the H versus time curve. A useful quantity for the quantitative assessment of phase change is the strain rate of dissipation energy density defined as

$$\frac{\Delta\mathcal{D}}{\Delta\varepsilon} \rightarrow \frac{\Delta Q}{\Delta V} \tag{20}$$

which reduces to $\Delta Q/\Delta V$ only as a special case. The values of $\Delta Q/\Delta V$ corresponding to the onset of phase change for metals can be found in handbooks.

*Heat transfer by radiation, convection and conduction will all be included in $\mathcal{D}$. There is no need to invoke assumptions on the way with which heat and temperature or temperature gradient are connected.

III. PROBLEM STATEMENT AND RESULTS

Suppose that a tungsten projectile traveling at 9,000 m/sec or 30,000 ft/sec comes in contact with a 5083 aluminum target plate as shown in Figure 3. Depending on the time interval at which the physical event is being reviewed, the material will undergo deformation, damage, phase transition, etc. The application of the energy density theory involves finding the dis-

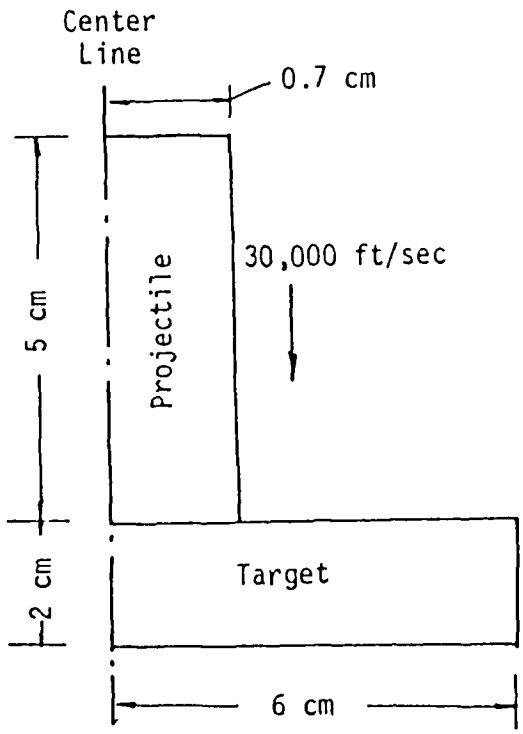

Figure 3. Hypervelocity Impact of Projectile/Target System

placements that yield the strain field from which the plane of homogeneity can be located. Unlike classical continuum mechanics, the tractions and inertia forces will interact as the rate change of volume with surface is no longer assumed to vanish, i.e.,

$$\overset{n}{T}_i = \sigma_{ij} n_j + \rho \frac{\partial^2 u_i}{\partial t^2} \left(\frac{dV}{dA}\right)_n \qquad (21)$$

in which ρ is the mass density and n the normal to the plane on which the tractions $\overset{n}{T}_i$ prevail. Here, σ_{ij} are the stress components that can be related to the strain function for each strain state through λ. The displacement components are denoted by u_i. It is important to recognize that even though $(dV/dA)_n$ in equation (21) may be small, the term $\rho\ \partial^2 u_i/\partial t^2$ may be large in dynamic problems

3.1 Initial Material Response

As remarked earlier, only a knowledge of the initial mechanical and thermal properties is required. They are outlined in Table 1 for the tungsten projectile and 5083 aluminum target. The quantities in Table 1 will be defined as the discussion proceeds.

TABLE 1. Reference Mechanical and Thermal Properties of Projectile and Target

Parameter	Tungsten	5083 Aluminum
E(GPa)	345	64.2
σ_{ys}(MPa)	1,062	132.5
σ_f(MPa)	1,347	260.8
$(dW/dV)_c$(MPa)	15.03	9.89
$(dW/dA)_c$(N/m)	6.18×10^4	2.09×10^5
ρ(kg/m^3)	19,350	2,700
C_p(J/kg°K)	145.7	900
T_m(°K)	3,683	1,200
ΔQ(J/kg)	4.93x105	8.10×10^5
$\Delta Q/\Delta V$(Pa)	9.64×10^7	2.21×10^7

For the sake of illustration, Figures 4 and 5 display the family of

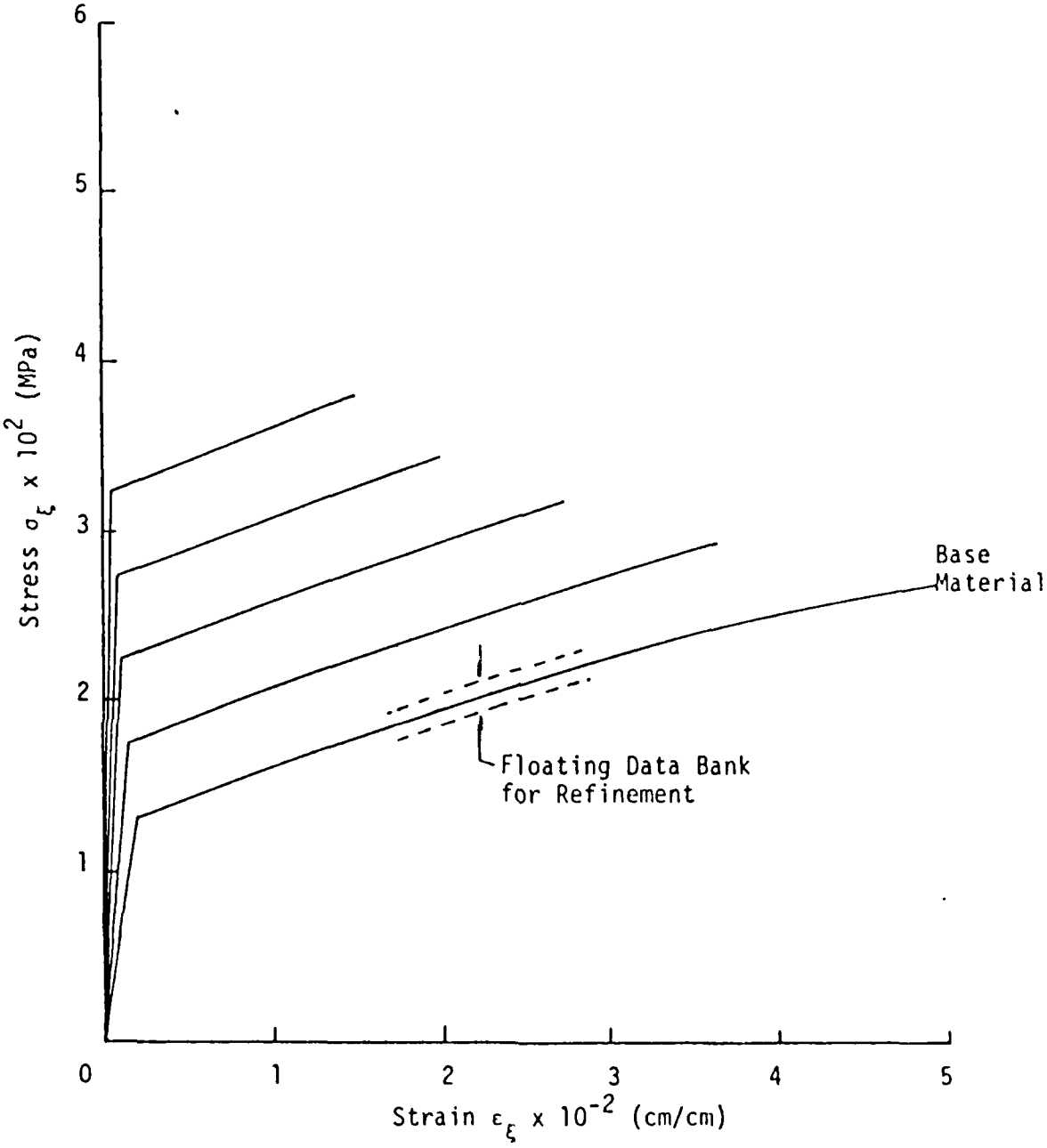

Figure 4. Stress and Strain Data Bank for Tungsten Projectile

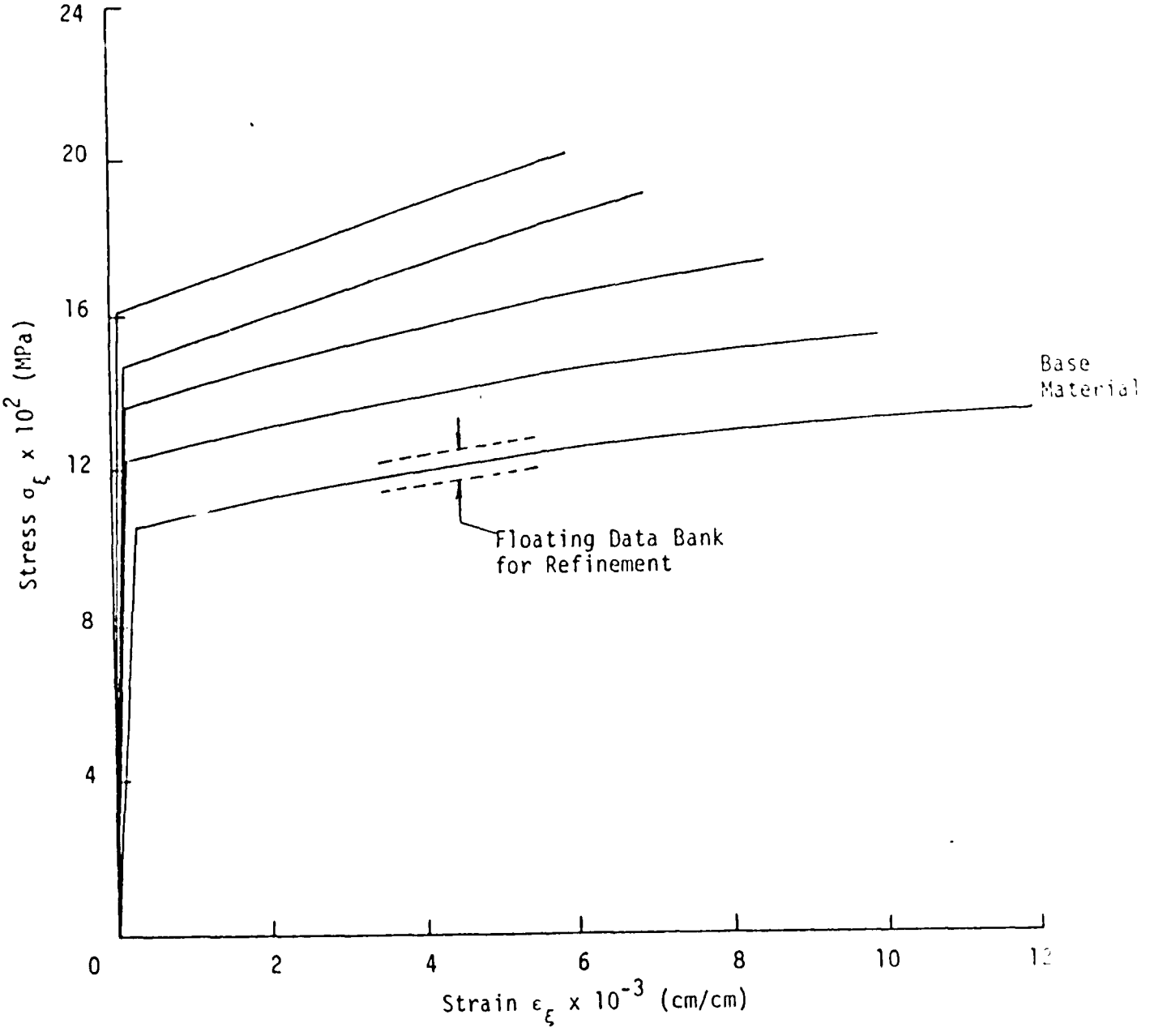

Figure 5. Stress and Strain Data Bank for 5083 Aluminum Target

stress and strain curves* for tungsten and 5083 aluminum as the strain rates are varied. They are referred to as the material data bank such that the base material serves as the reference state. Refinement of the data can be achieved by introducing a floating bank to the desired degree of accuracy. The idea is that each point $(\sigma_\xi, \varepsilon_\xi)$ on the plane of homogeneity can be uniquely and accurately identified with a uniaxial stress and strain state or $[(dV/dA)_\xi, \varepsilon_\xi]$. The actual response of a given element in the projectile/target system may not coincide with any of the curves shown in Figures 4 and 5. It will most likely follow a path that intersects the curves at several points because the probability of any elements deforming at a constant strain rate under impact is small. As it will be shown subsequently, the stress and strain curves for elements near the region of impact will in no way resemble those in Figures 4 and 5 for tungsten and aluminum in the solid state. In fact, they will behave as viscous fluid because local melting has occurred. This is illustrated in Figure 6 where the initial responses of the projectile and target material are covered by the family of linear curves. The dotted line is the actual response of an element in the fluid state determined automatically. Phase transition is accounted for by the energy density theory. There is no need to guess or anticipate the form of the constitutive relations as required in the classical approach. The shapes of the stress and strain curves selected in the material data bank are not essential as long as all the points in the σ_ξ versus ε_ξ domain are uniquely identified with $[(dV/dA)_\xi, \varepsilon_\xi]$. The objective is to mathematically establish an one-to-one correspondence between the stress and/or strain state of each element and its equivalent

*Each curve refers to a different strain rate.

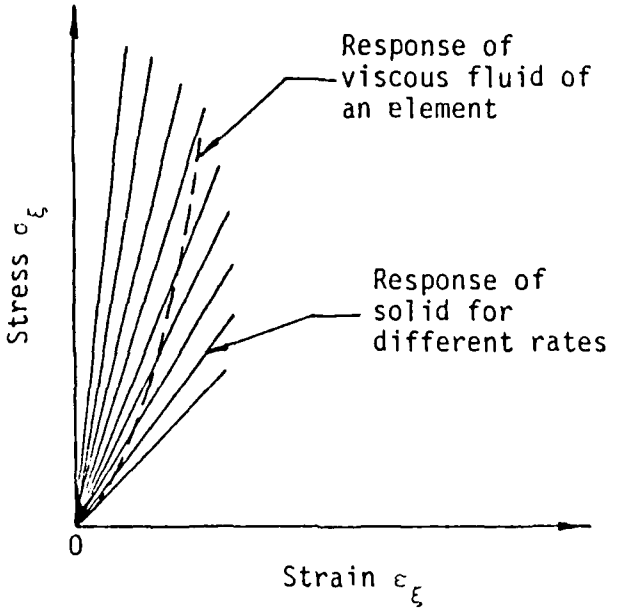

Figure 6. Response of Viscous Fluid Determined From Material Data Bank For Solid

uniaxial state. It is simply a bookkeeping procedure. There is no longer the need to obtain uniaxial data for different strain rates* except for the initial response to be used as a reference. *The energy density theory can analytically determine the complete stress and strain behavior for any strain rates from only a knowledge of the initial Young's modulus and the specified loading rate.* This has been done for the 6061-T6 aluminum stretched uniaxially at a strain rate of 10^{-3} and 10^{-4} sec^{-1} and the prediction is within 5% of the experimental data [8].

3.2 Image Mapping

The projectile/target system is discretized by application of the twelve (12) node isoparametric finite elements. Since the geometry in Figure 1

*For strain rates of 10 sec^{-1} and higher considerable difficulties are encountered experimentally in uniaxial tests. A review of the subject can be found in [7].

possesses one-half symmetry, it suffices to use 20 elements and 138 nodes as indicated in Figure 7(a). As the boundary conditions along the plane of symmetry cannot always be adequately satisfied numerically, the method of image mapping will be adopted. Sixteen additional elements are added that simply reflects the displacement field symmetrically across the center plane, Figure 7(a). This will obviously provide more accurate results for elements no. 15 and 17. Particular attention will be given to the results at points 1, 2 and 3 in the target and 4, 5 and 6 in the projectile, Figure 7(b). All quantities referred to these locations will be averaged over a circular region with diameter 0.02 cm. Computed are dW/dV and dW/dA contours in the projectile/target system for different time increments. Figure 8 displays the volume energy density contours at t = 2 nsec. The contours are seen to be densely packed near the corner with increasing magnitude. This is not surprising because reentrant corners tend to concentrate energy. Even at this very early stage of contact, energy has transferred to all elements in the target. There prevails a five order of magnitude difference in the intensity of the twenty one (21) dW/dV contours displayed in Figure 8. Similarly, the surface energy density contours can also be plotted as given in Figure 9 at t = 2 nsec. Their distribution is similar to that of dW/dV in Figure 8. The spread in the difference of the intensity of dW/dA, however, has increased by one order of magnitude, i.e., the value of dW/dA for contour no. 1 differed from that of no. 21 by six order of magnitude. The surface energy density is expected to dominate at initial impact because energy is transmitted across the contact surface between the project and target before it can spread volume wise. An enlarged view of the dW/dA contours near the corner is shown in Figure 10. This provides an insight into the shape of local region within

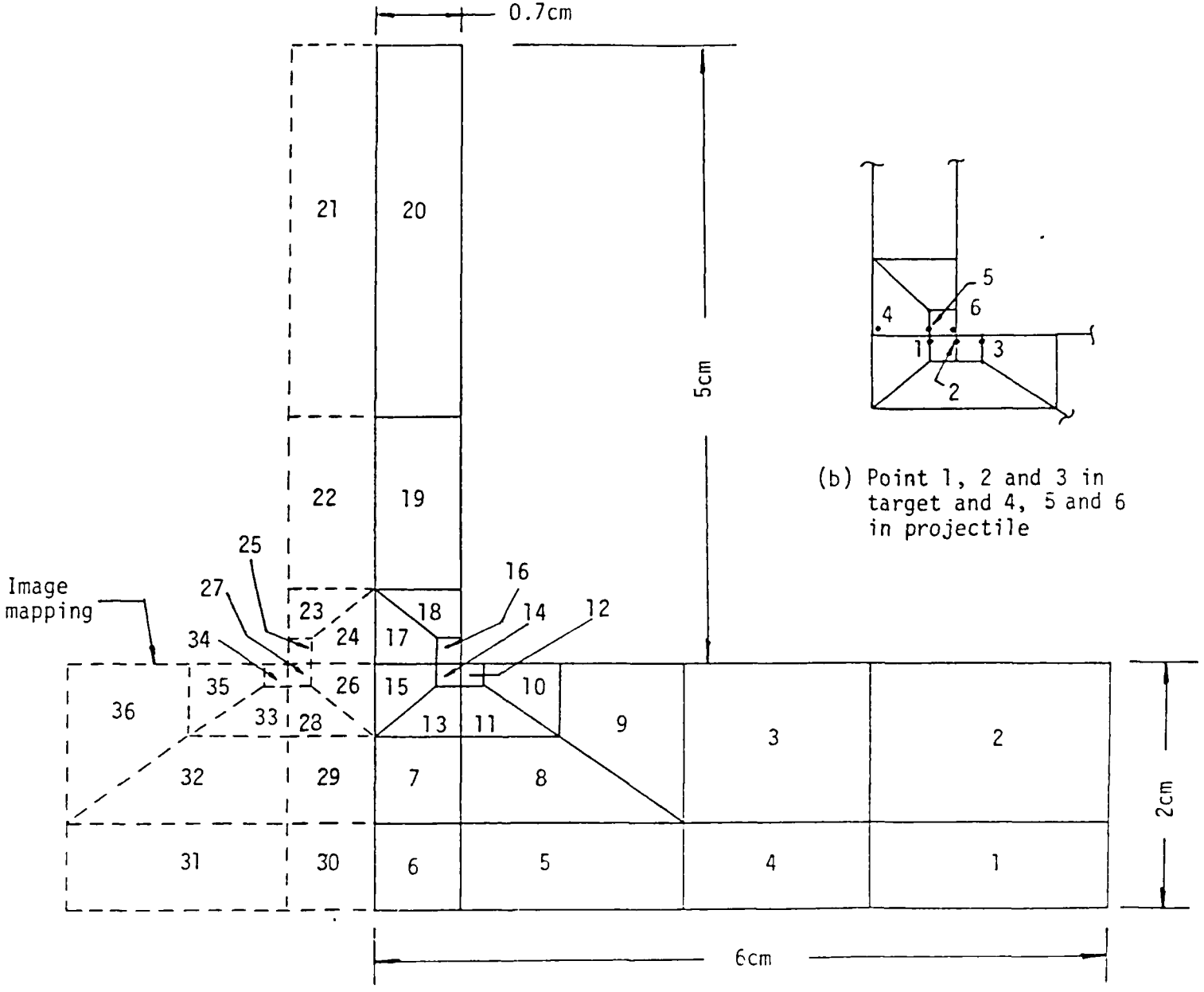

(a) Numbering of elements

(b) Point 1, 2 and 3 in target and 4, 5 and 6 in projectile

Figure 7. Grid Pattern for Projectile/Target System With Image Mapping

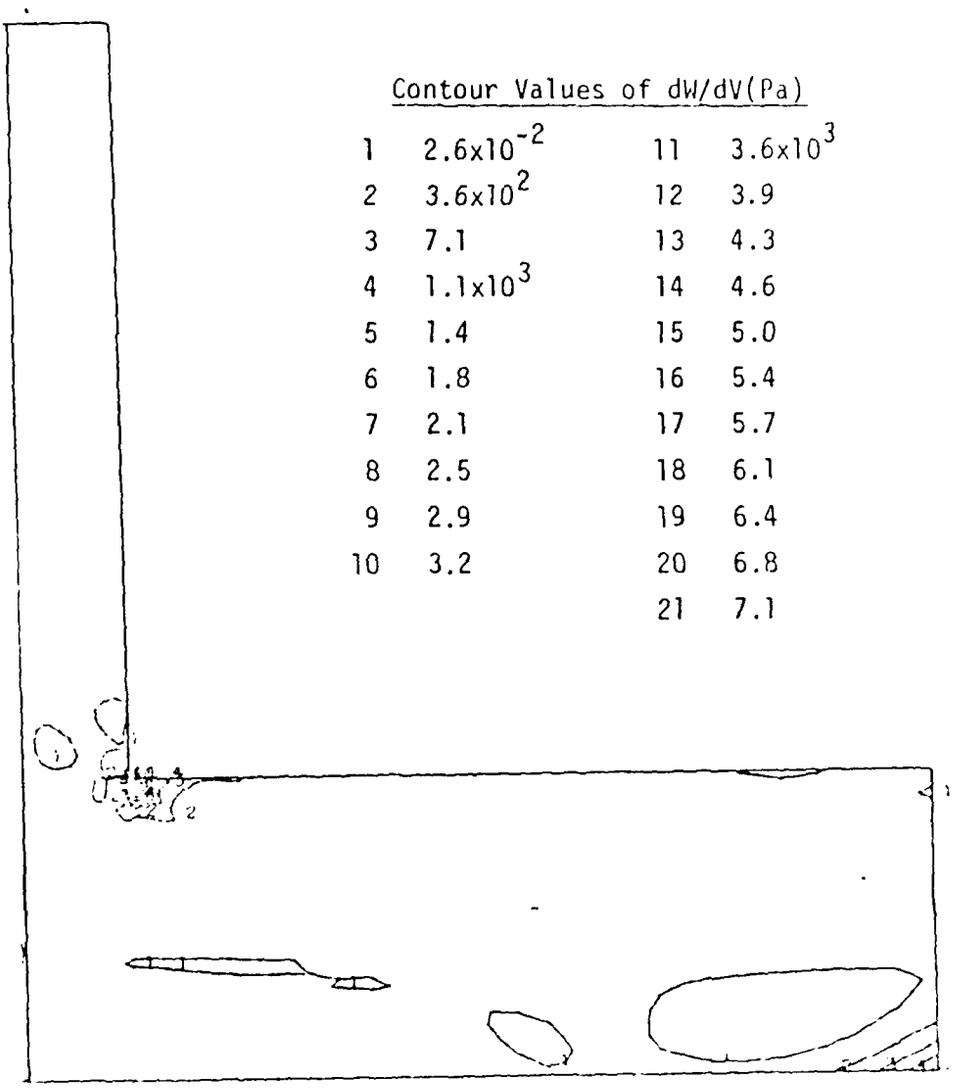

Contour Values of dW/dV(Pa)

1	2.6×10^{-2}	11	3.6×10^{3}
2	3.6×10^{2}	12	3.9
3	7.1	13	4.3
4	1.1×10^{3}	14	4.6
5	1.4	15	5.0
6	1.8	16	5.4
7	2.1	17	5.7
8	2.5	18	6.1
9	2.9	19	6.4
10	3.2	20	6.8
		21	7.1

Figure 8. Constant Volume Energy Density dW/dV at t = 2 nsec

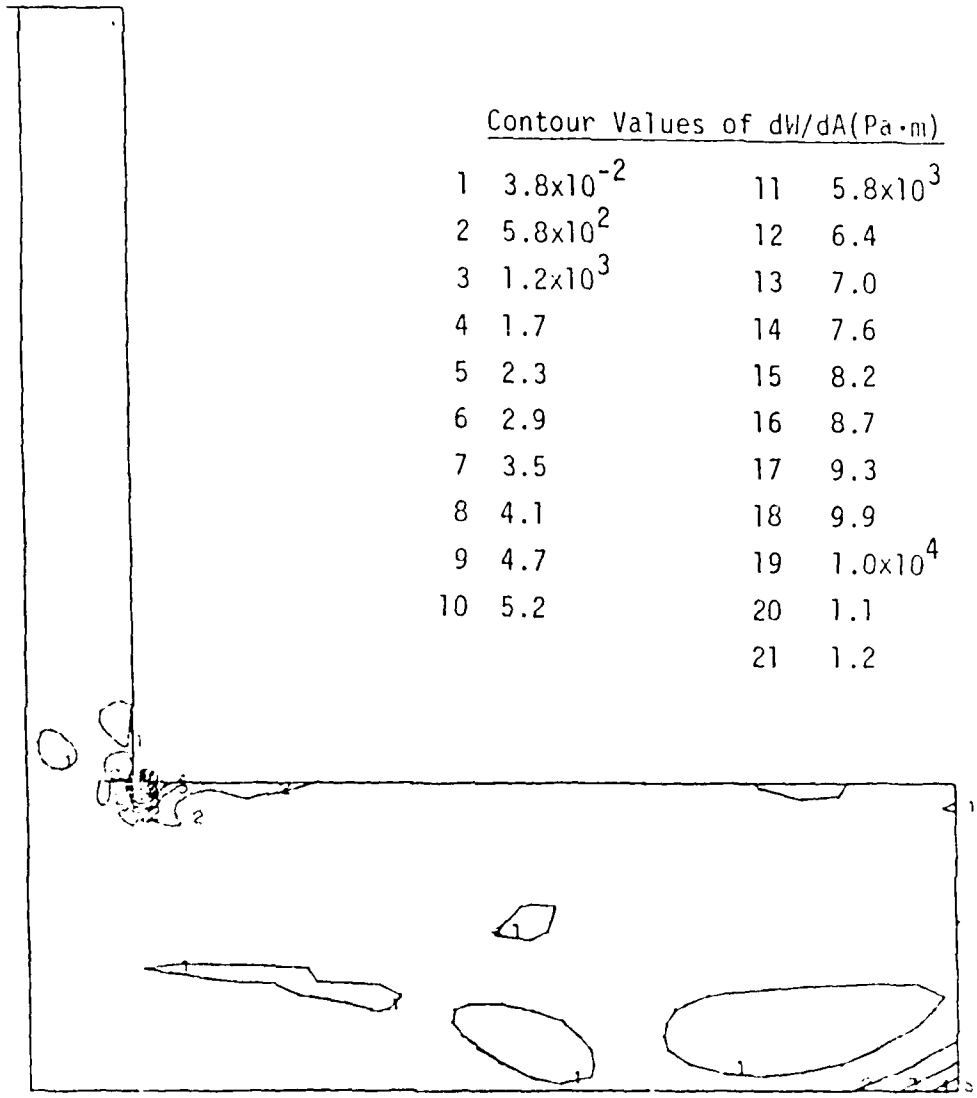

Figure 9. Constant Surface Energy Density dW/dA Contours at t = 2 nsec

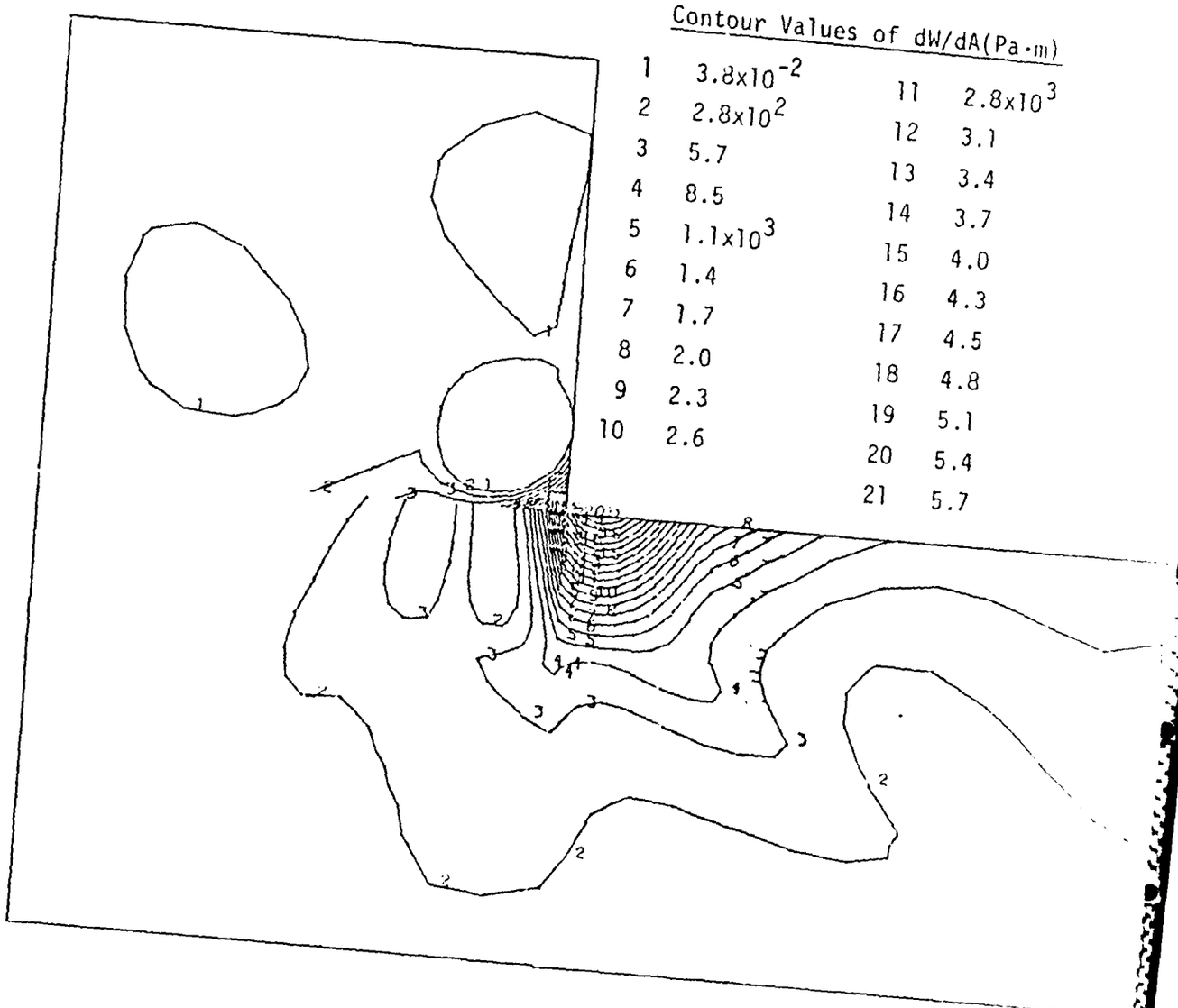

Figure 10. Constant Surface Energy Density dW/dA Contours in Enlarged Corner Region of Projectile/Target System At t = 2 nsec

which the material may change phase. As time elapses to t = 4 nsec, energy is being continuously transmitted from the projectile into the target. This is evidenced by the increase in the intensity of the dW/dV and dW/dA contours exhibited in Figures 11 and 12, respectively. An one order of magnitude increase in the volume and surface energy density can be observed. Concentration of energy remains in the vicinity of the corner. Figure 13 gives the details of the dW/dA contours for t = 4 nsec.

IV. SUB-SCALING OF PROJECTILE/TARGET SYSTEM

Prior to performing sub-scaling tests of projectile/target systems, it is necessary to establish the conditions or criteria under which geometric, kinematic, material, damage and time parameters are to be proportioned or scaled. Because energy dissipation during hypervelocity impact plays a dominant role, scaling of the aforementioned parameters will be highly non-linear. For the purpose of gaining insight into the physical problem, three different projectile/target systems will be analyzed.

4.1 Geometric Proportionality

Shown in Figures 14(a), 14(b) and 14(c) are three different projectile/target systems which shall be referred to as full scale (1:1), half scale (1:2) and quarter scale (1:4), respectively. Geometric proportionality is assumed such that

$$\frac{A}{B} = \frac{a}{b} = \frac{\alpha}{\beta} \quad ; \quad \frac{C}{D} = \frac{c}{d} = \frac{\gamma}{\delta} \tag{22}$$

The masses m_p, m_h, m_q and velocities v_p, v_h, v_q can alter depending on the

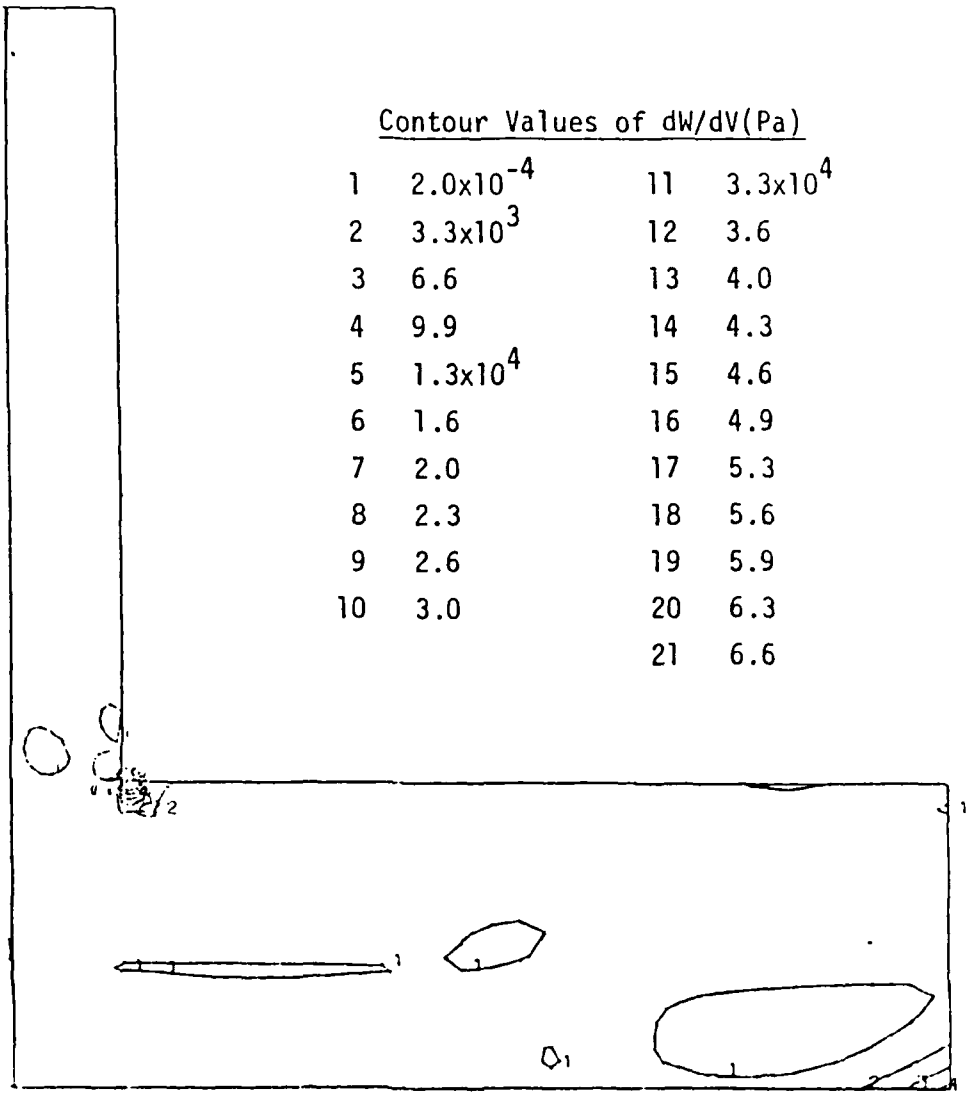

Figure 11. Constant Volume Energy Density dW/dV At t = 4 nsec

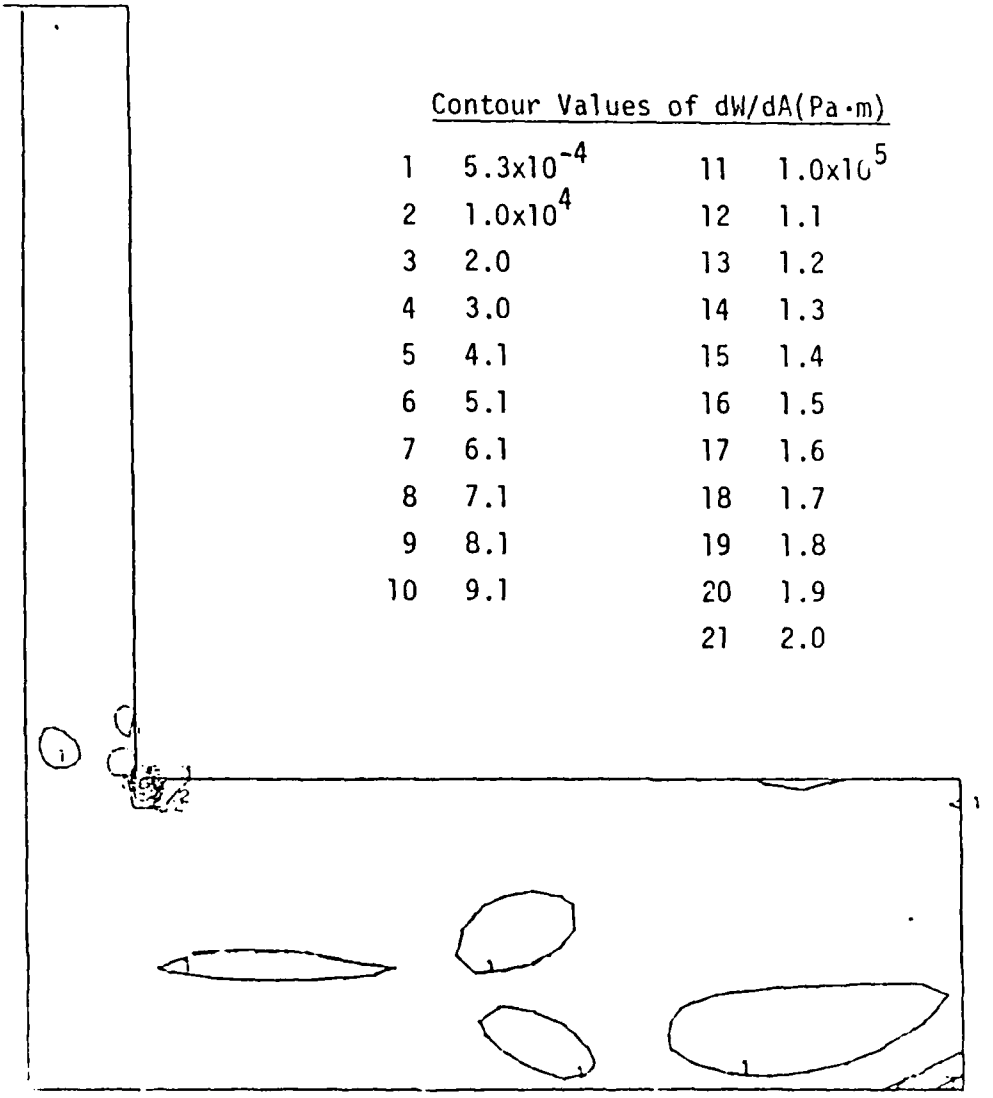

Figure 12. Constant Surface Energy Density dW/dA Contours At t = 4 nsec

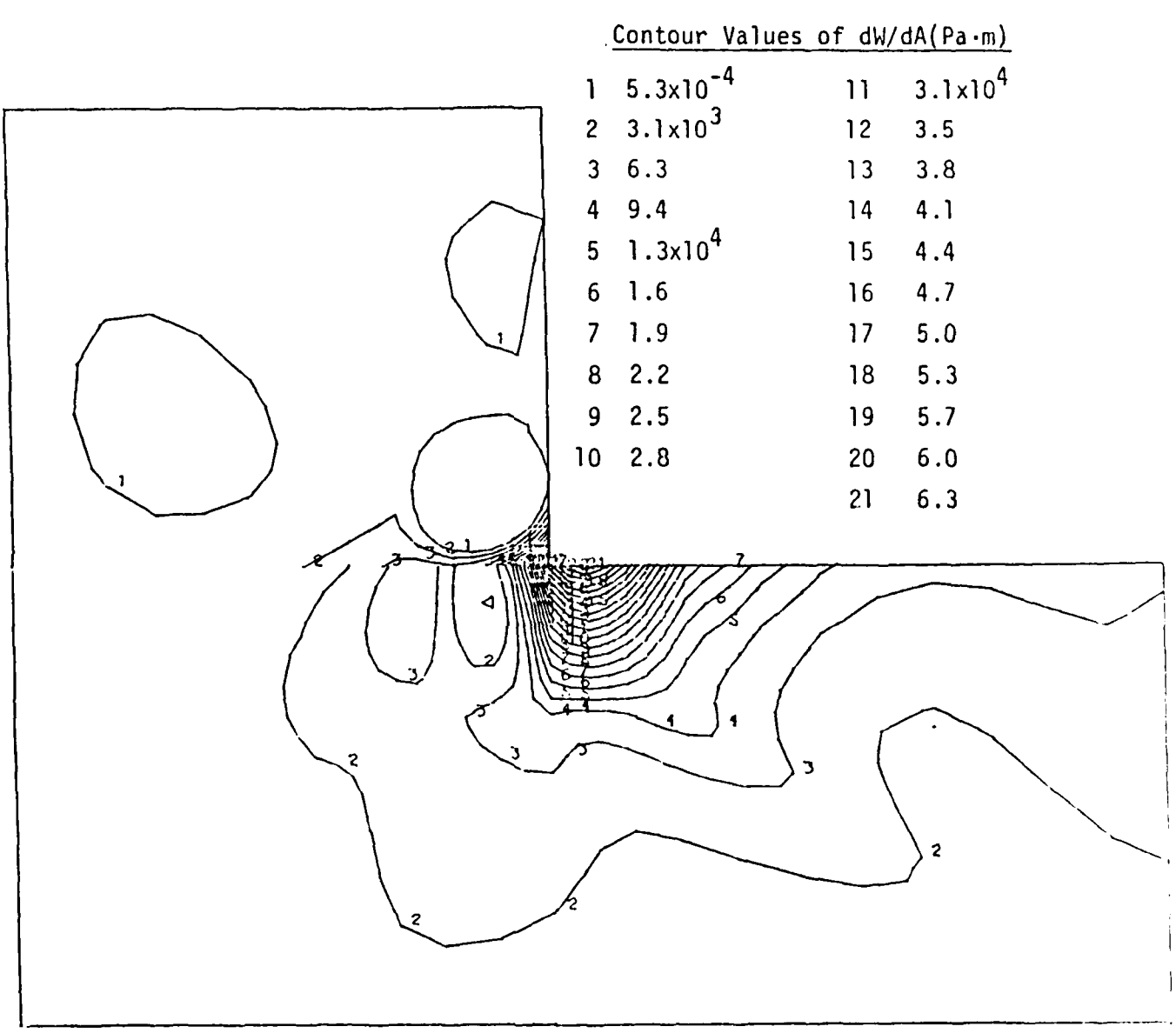

Figure 13. Constant Surface Energy Density dW/dA Contours On Enlarged Corner Region Of Projectile/Target System At t = 4 nsec

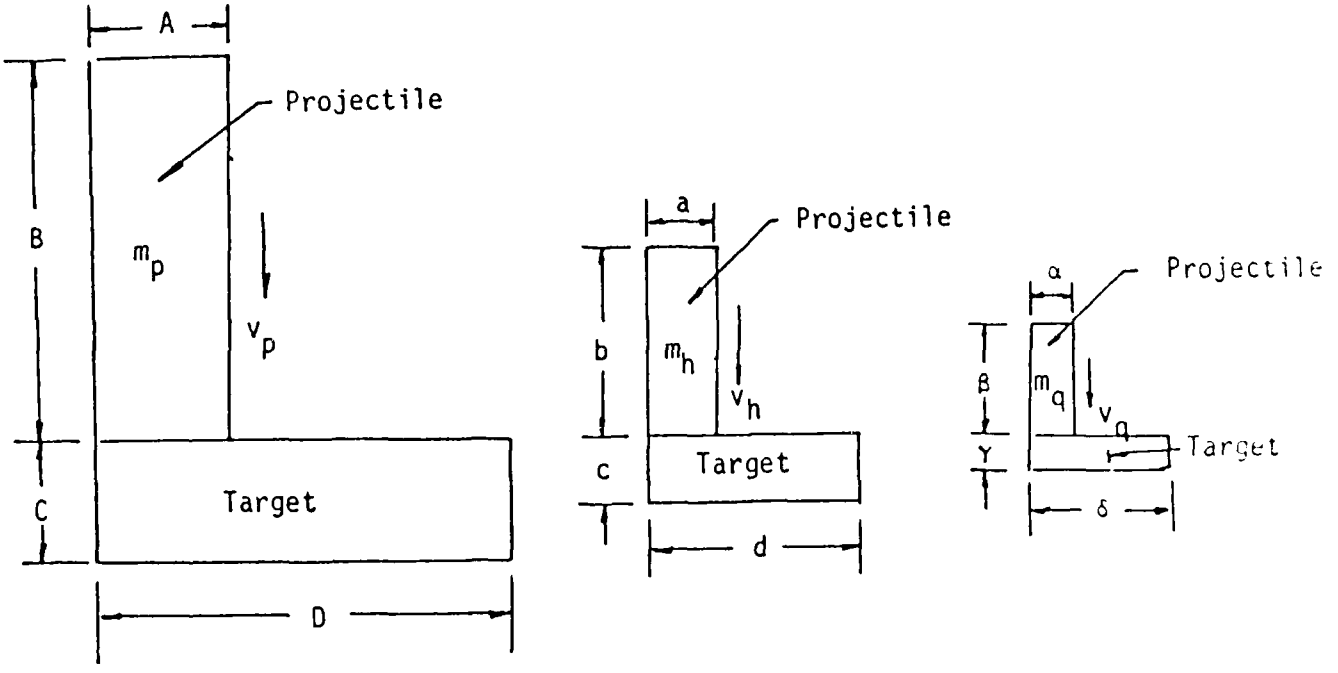

(a) Full scale (1:1) (b) Half scale (1:2) (c) Quarter Scale (1:4)

Figure 14. Sub-scaling of Projectile Target System

extent with which kinetic energy and/or momentum change affect material damage.

Suppose that the systems in Figures 14(a) to 14(c) are scaled to preserve the kinetic energy in addition to satisfying the conditions in equation (22). This then requires

$$\frac{1}{2} m_p v_p^2 = \frac{1}{2} m_h v_h^2 = \frac{1}{2} m_q v_q^2 \qquad (23)$$

for the initial time step. Solving for the velocities of the sub-scale system in terms of the full scale projectile velocity, it is found that

$$v_h = \left(\frac{m_p}{m_h}\right)^{0.5} v_p \quad , \quad v_q = \left(\frac{m_p}{m_q}\right)^{0.5} v_p \tag{24}$$

On the other hand, if momentum is to be conserved then

$$m_p v_p = m_h v_p = m_q v_q \tag{25}$$

This yields

$$v_h = \left(\frac{m_p}{m_h}\right)^{1} v_p \quad , \quad v_q = \left(\frac{m_p}{m_q}\right)^{1} v_p \tag{26}$$

In practice, the exponent on the mass ratio will neither be 0.5 or 1.0. That is geometric proportionality will not conserve the projectile kinetic energy or momentum. At any given instance of time, there will be a two parameter scaling relation of the form

$$v_h = k_1 \left(\frac{m_p}{m_h}\right)^{n_1} v_p \tag{27}$$

for the half-scale system and

$$v_q = k_2 \left(\frac{m_p}{m_q}\right)^{n_2} v_p \tag{28}$$

for the quarter-scale system. The quantities k_1, k_2 and n_1, n_2 will depend on the damage in the projectile/target system that changes with time.

4.2 Response in Target

If the three systems in Figures 14(a) to 14(c) are to experience approxi-

mately the same damage at a given time,* then the velocities v_h and v_q must be scaled accordingly. After several trial runs, the initial velocities for the half scale and quarter scale model in Table 2 were chosen. They are lower than that of the full scale system. Otherwise, the scaled down target will experience more damage at a given time. For the *same material*, the energy concentration will be more severe for the smaller projectile/target system because the distance between the corners are reduced. Figures 15, 16 and 17 show the variations of compressive stress σ_ξ with compressive

TABLE 2. Projectile Velocity at t = 4 nsec for Different Scaled Models

Scale	Initial Velocity (m/sec)	Velocity at t = 4 nsec (m/sec)
Full (1:1)	9,000	8,526.7
Half (1:2)	4,000	3,836.5
Quarter (1:4)	1,800	1,690.0

strain ε_ξ for the full scale, half scale and quarter scale system at t = 4 nsec at points 1, 2 and 3 as indicated in Figure 7(b), respectively. The response corresponds to that for viscous fluid. Point 2 being directly under the periphery of the projectile experiences higher stress and strain. Next in line is point 3 which is near the free surface of the target. The terminal points of the σ_ξ versus ε_ξ curves in Figures 16 and 17 can be elevated closer to those in Figure 15 for the full scale system if the initial velocities v_h and v_q in Table 2 are increased accordingly. Only the initial response of the base material were used to obtain the results in Figures 15 to 17. The corresponding numerical values are given in Table 3 for t = 2 and 4 nsec.

*Refer to detailed discussion in Section V.

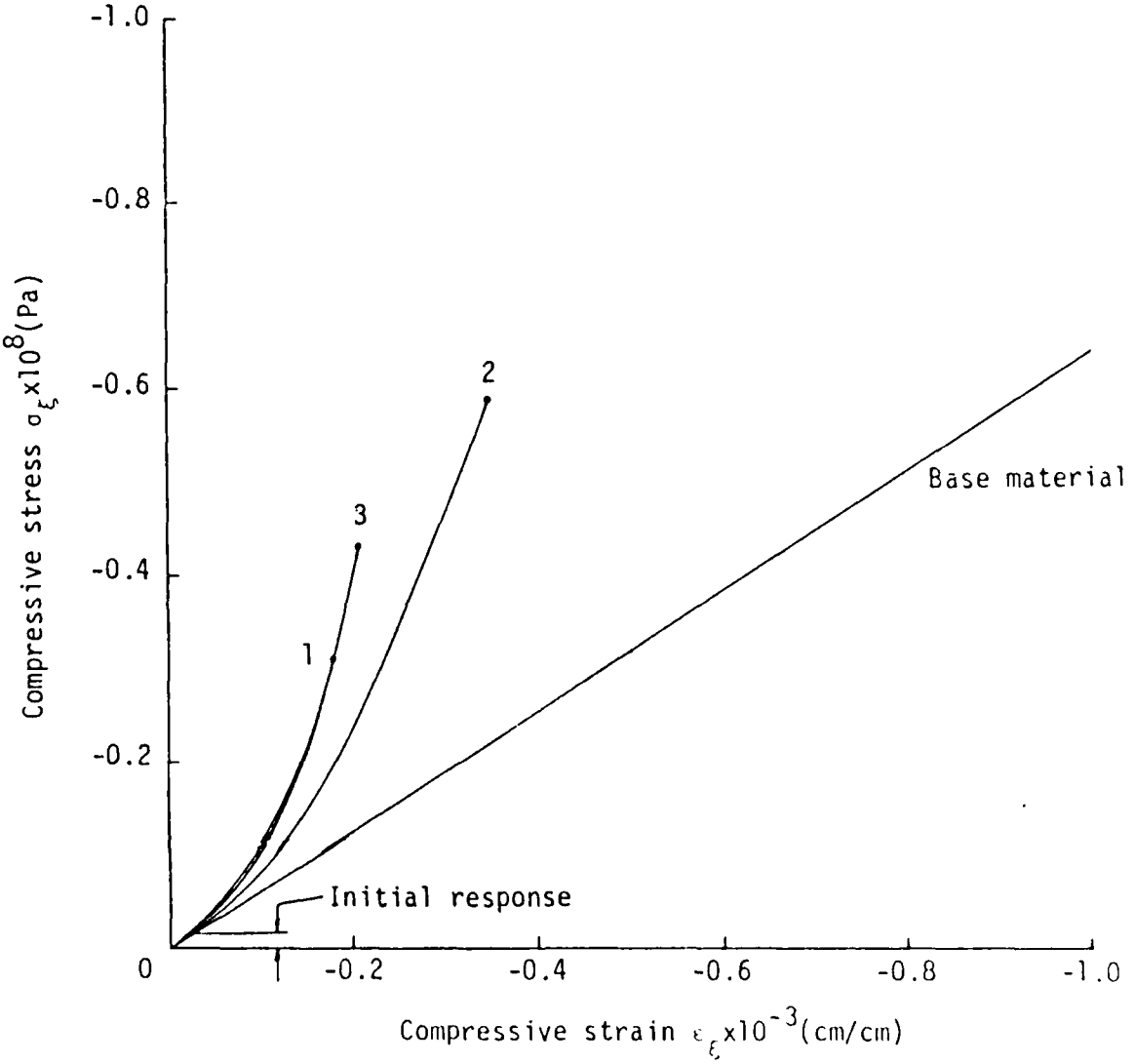

Figure 15. Stress And Strain Response At Point 1, 2 And 3 In Target for t = 4 nsec And Full Scale(1:1)

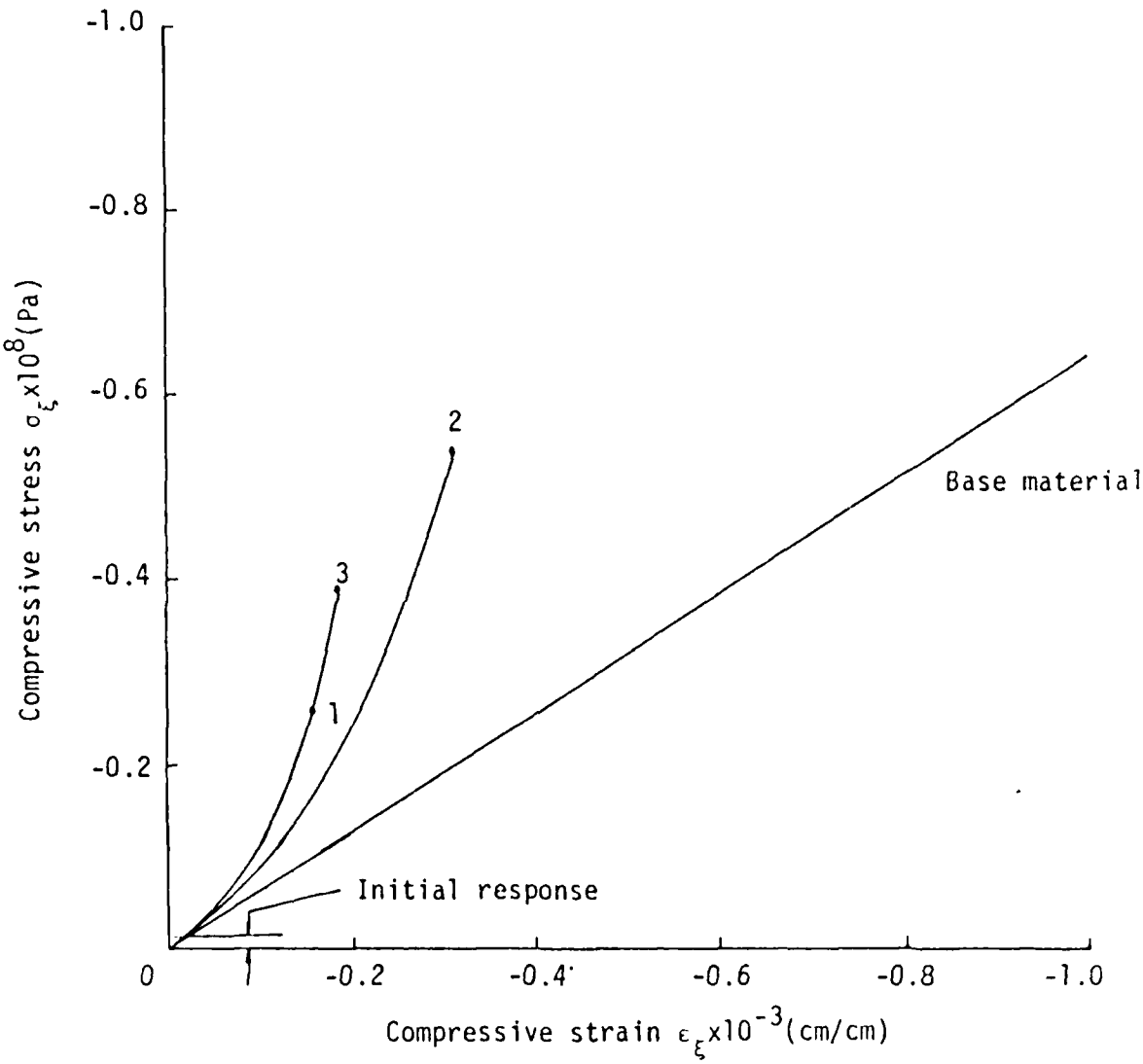

Figure 16. Stress and Strain Response At Point 1, 2 And 3 In Target For t = 4 nsec And Half scale (1:2)

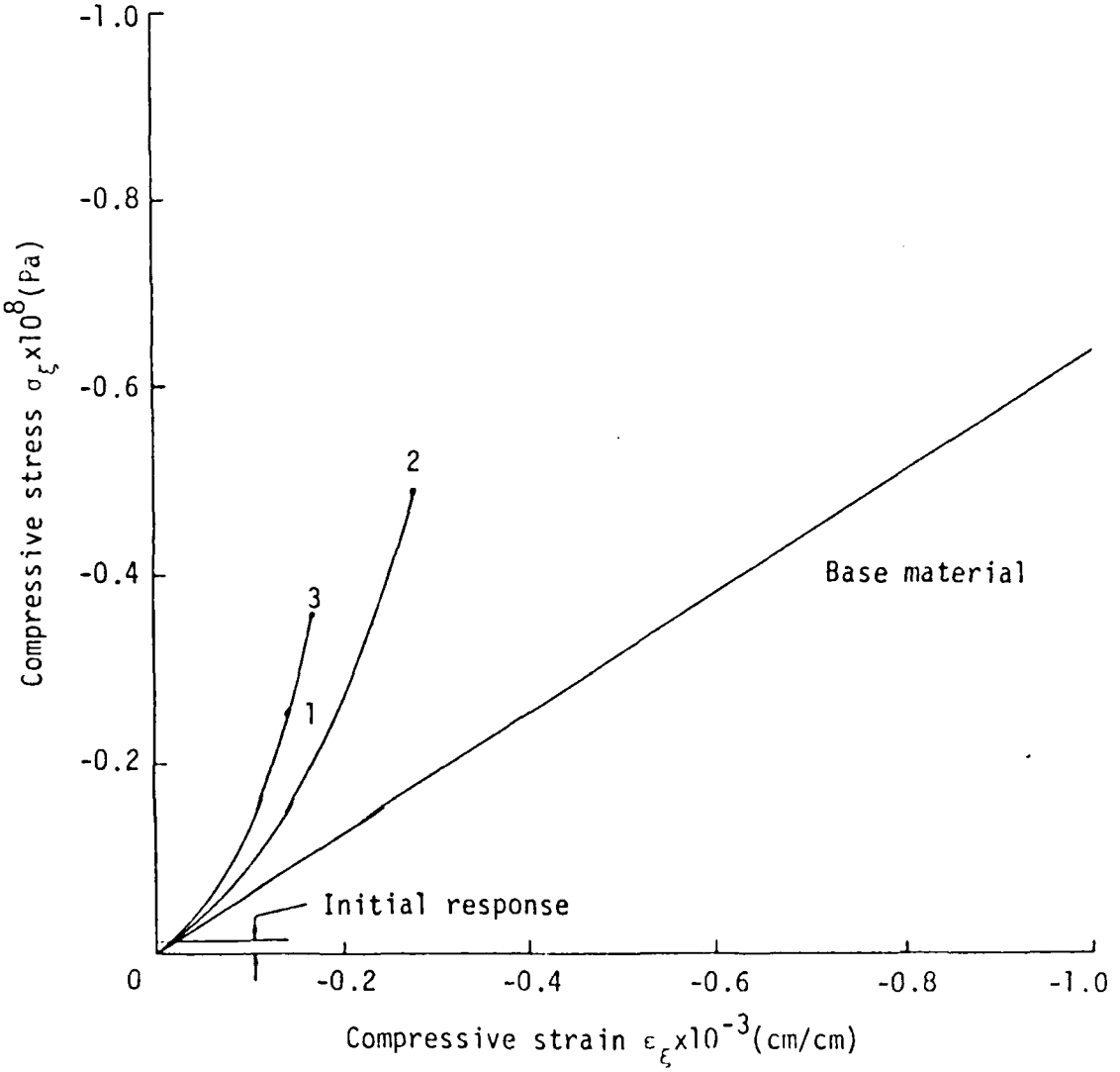

Figure 17. Stress And Strain Response At Point 1, 2 And 3 In Target For t = 4 nsec And Quarter Scale (1:4)

TABLE 3. Stress and Strain on Plane of Homogeneity at Point 1, 2 and 3 in Target

Time t(nsec)	Point 1 $\varepsilon_\xi \times 10^{-3}$ (cm/cm)	Point 1 $\sigma_\xi \times 10^{8}$ (Pa)	Point 2 $\varepsilon_\xi \times 10^{-3}$ (cm/cm)	Point 2 $\sigma_\xi \times 10^{8}$ (Pa)	Point 3 $\varepsilon_\xi \times 10^{-3}$ (cm/cm)	Point 3 $\sigma_\xi \times 10^{8}$ (Pa)
Full Scale (1:1)						
2	-0.08965	-0.08745	-0.1758	-0.1829	-0.1134	-0.1303
4	-0.1824	-0.3056	-0.3533	-0.5994	-0.2117	-0.4324
Half Scale (1:2)						
2	-0.07969	-0.07813	-0.1563	-0.1634	-0.1008	-0.1164
4	-0.1622	-0.2745	-0.3142	-0.5384	-0.1882	-0.3883
Quarter Scale (1:4)						
2	-0.07172	-0.07095	-0.1407	-0.1484	-0.09069	-0.1057
4	-0.1460	-0.2516	-0.2827	-0.4934	-0.1694	-0.3559

By determining the path of local unloading, the available energy density can be distinguished from the dissipation energy density for each load step. The quantity D as defined in equation (10) can thus be found. Keeping in mind that D and dD/dt must be positive*. The correct feature and trend of D is shown in Figures 18(a) to 18(c) for the three different systems. Point 2 dissipates more energy at t = 4 nsec than points 1 and 3. This trend remains valid for t = 2 nsec as given in Table 4. Once the time history of D is known, ΔD in equation (19) follows immediately. With the aid of the data in Table 3 for σ_ξ and ε_ξ, the temperature θ in equation (18) can be calculated. The results are plotted as a function of time in Figures 19(a) to 19(c) with θ_0 being

*These conditions may not be satisfied on the first trial. Readjustment of the finite element grid size compatible with the time increment is frequently necessary. The optimum choice corresponds to diminishing oscillation of D with time for small t.

equal to 300°K. Even though all three points 1, 2 and 3 are beyond the melting temperature Θ_m = 1,200°K for the 5083 aluminum, the strain rate of energy dissipation density $\Delta D/\Delta\varepsilon$ should be checked to see whether the material elements at points 1, 2 and 3 have indeed melted or not. Refer to Table 5 for the numerical values of Θ-Θ_0. It is conceivable that $\Delta D/\Delta\varepsilon$ corresponding to a unit volume of material* may pass the threshold of melting only momentarily and then drops below its critical value. According to the results in Table 4, this is not the case. But rather, $\Delta D/\Delta\varepsilon$ at points 2 and 3 increased monotonically with time as it passes the threshold $\Delta Q/\Delta V = 22.1 \times 10^6$Pa as given in Table 1 for the 5083 aluminum. Point 1 remains below the melting condition even though its temperature is near the melting point. The transition of solid to fluid for a unit volume of material is guaranteed when both Θ and $\Delta D/\Delta\varepsilon$ are maintained beyond the critical level within a certain time period.

To be noted is that at the very early stage of impact, the phenomenon of cooling and heating also occurs although its influence is negligible in comparison with the time history of the total impact process. This is similar to that observed in [2,3] for metal specimens loaded uniaxially at low strain rates.

4.3 Response in Projectile

Upon impact, the elements in the projectile also experiences compressive stress and compressive strain. Referring to the plane of homogeneity, the σ_ξ versus ε_ξ relations for points 5 and 6 at t = 4 nsec are plotted in Figures 21, 22 and 23. They represent, respectively, the full scale, half scale and quarter scale as shown in Figures 14(a), 14(b) and 14(c). Again,

*A unit volume of material ΔV used to calculate $\Delta D/\Delta\varepsilon$ corresponds to a local region 0.02 cm in diameter.

TABLE 4. Dissipation Energy Density and Strain Rate Dissipation Energy Density at Point 1, 2 and 3 in Target

Time t(nsec)	Point 1		Point 2		Point 3	
	$\mathcal{D}\times10^3$ (Pa)	$\Delta\mathcal{D}/\Delta\varepsilon\times10^6$ (Pa)	$\mathcal{D}\times10^3$ (Pa)	$\Delta\mathcal{D}/\Delta\varepsilon\times10^6$ (Pa)	$\mathcal{D}\times10^3$ (Pa)	$\Delta\mathcal{D}/\Delta\varepsilon\times10^6$ (Pa)
Full Scale (1:1)						
2	0.1625	4.12	0.6496	6.09	0.3259	5.43
4	1.3143	19.96	4.6087	38.20	1.9972	33.52
Half Scale (1:2)						
2	0.1303	3.66	0.5204	5.32	0.2605	4.77
4	1.0575	18.05	3.7091	34.79	1.6048	30.73
Quarter Scale (1:4)						
2	0.1083	3.43	0.4318	5.0	0.2154	4.46
4	0.8841	16.94	3.3982	32.28	1.3394	28.58

TABLE 5. *Temperature Change at point 1, 2 and 3 in Target*

Time t(nsec)	Point 1 $\theta-\theta_o$ (°K)	Point 2 $\theta-\theta_o$ (°K)	Point 3 $\theta-\theta_o$ (°K)
Full Scale (1:1)			
2	1,171	1,027	909
4	930	1,053	922
Half Scale (1:2)			
2	1,160	1,019	903
4	925	1,044	917
Quarter Scale (1:4)			
2	1,140	1,005	893
4	914	1,029	906

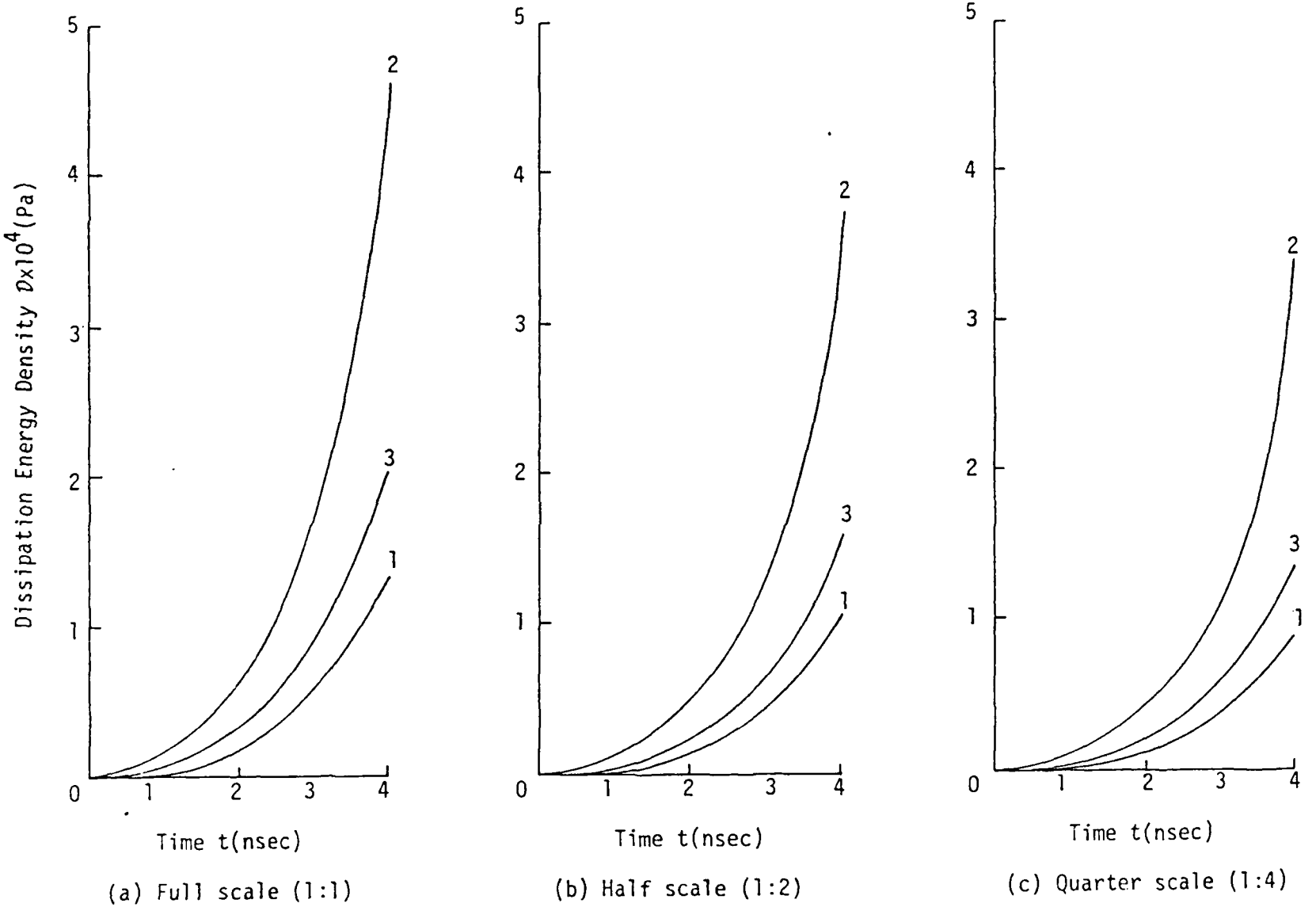

Figure 18. Time History of Dissipation Energy Density At Point 1, 2 And 3 In Target

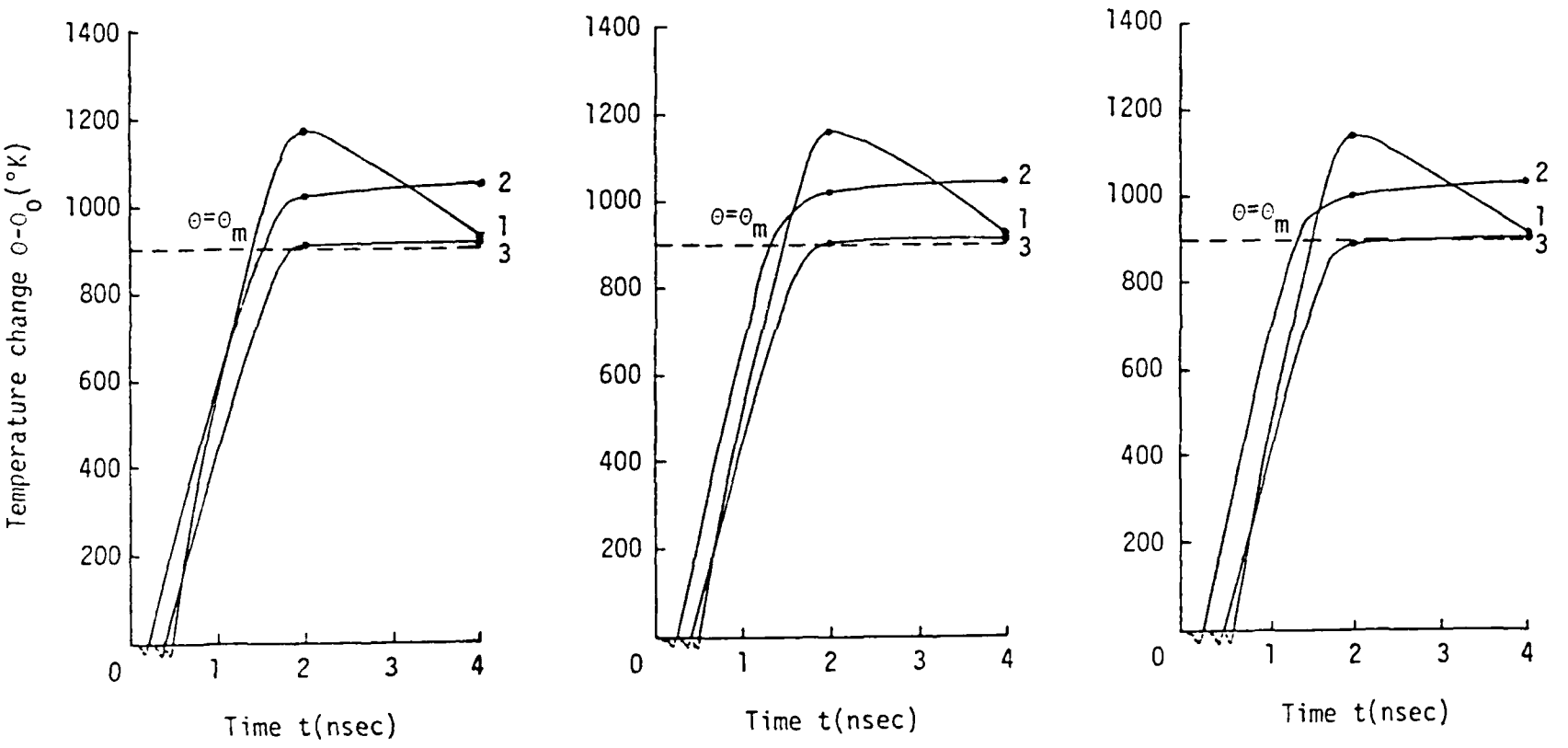

Figure 19. Time History Of Temperature Change At Part 1, 2 And 3 In 5083 Aluminum Target With Melting Temperature Of 1,200°K

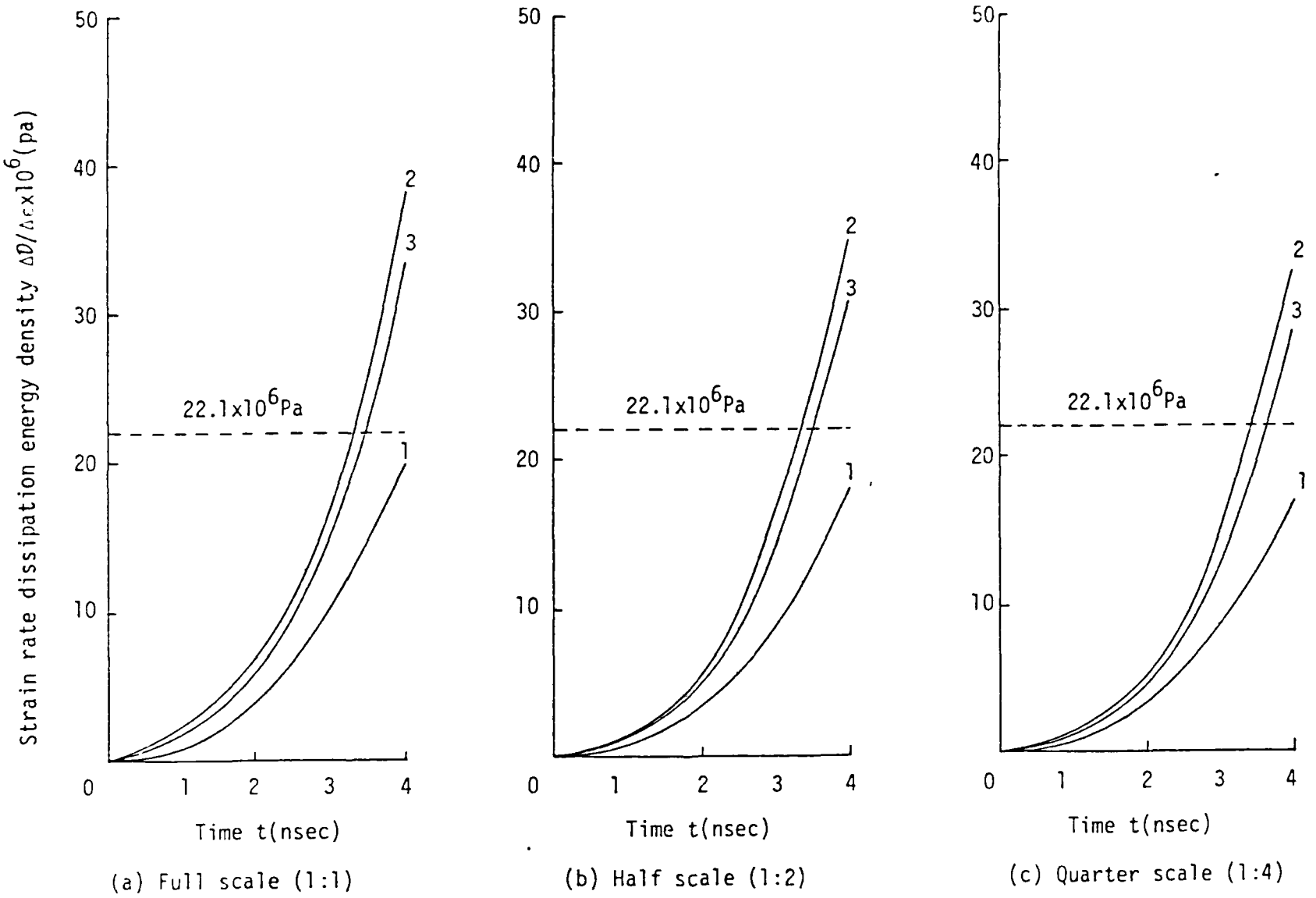

Figure 20. Time History of Strain Rate Energy Dissipation Energy Density At Point 1, 2 And 3 In Target

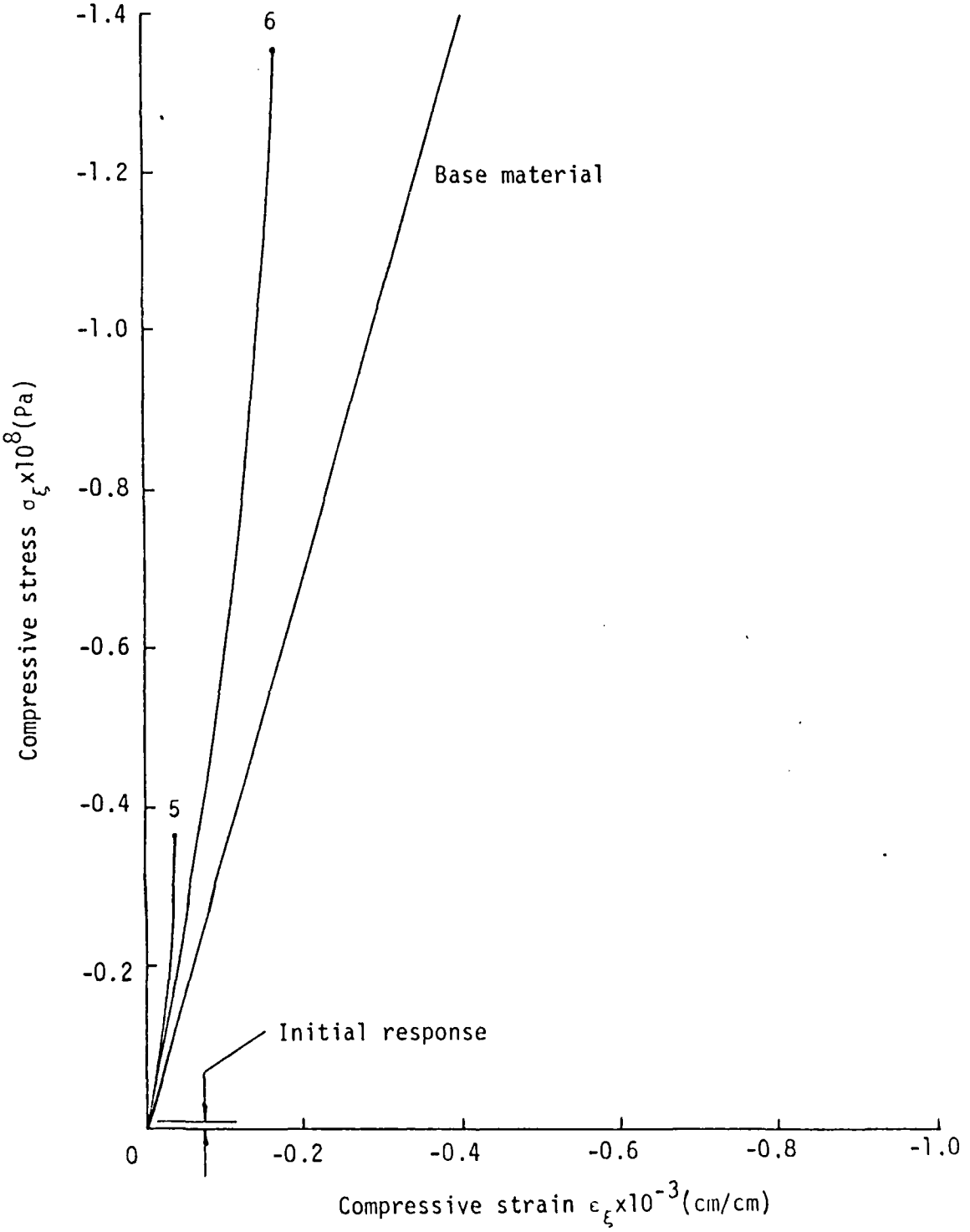

Figure 21. Local Stress And Strain Response At Point 5 and 6 in projectile for t = 4nsec And Full scale (1:1)

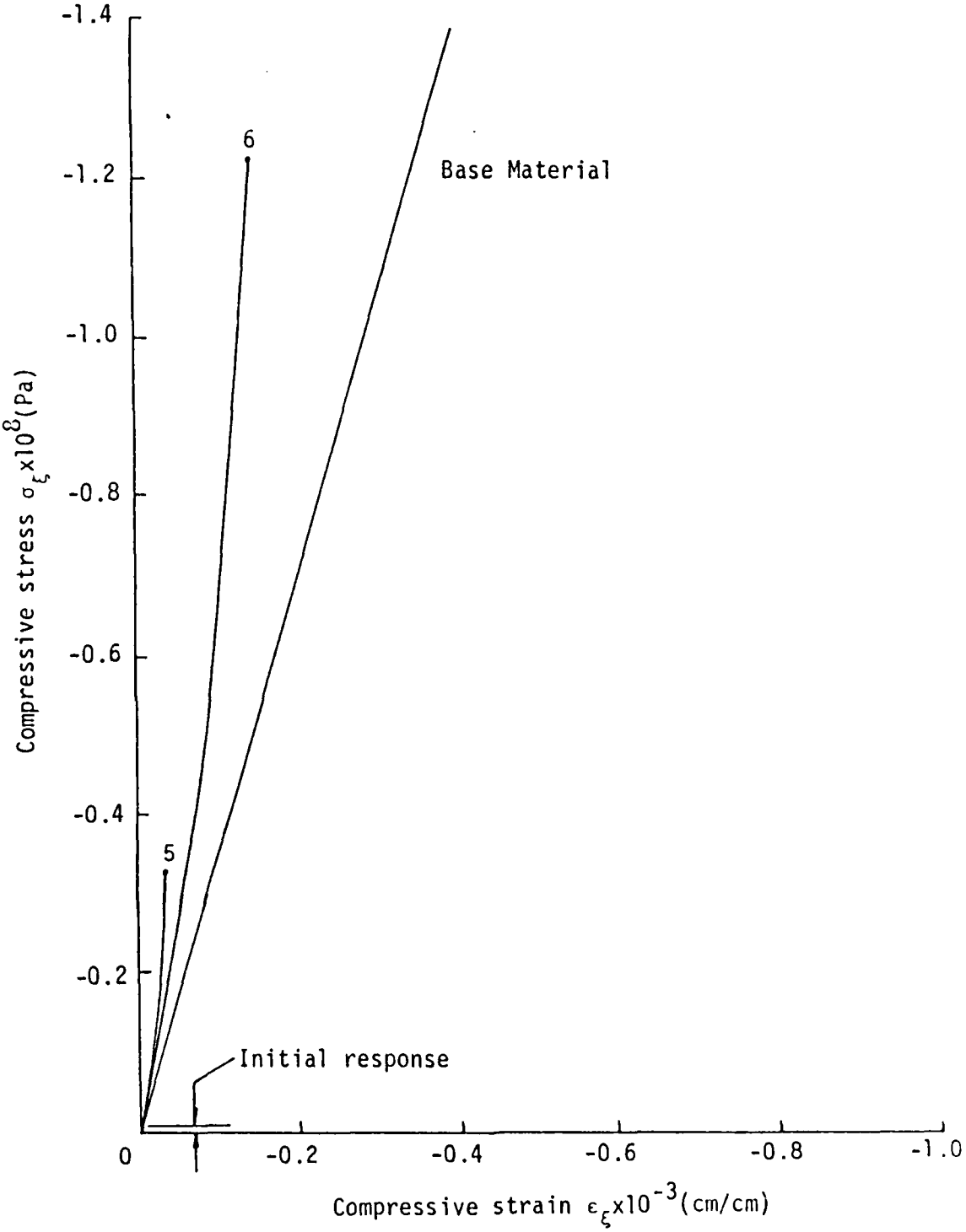

Figure 22. Local Stress And Strain Response At Point 5 And 6 In projectile For t = 4 nsec And Half Scale (1:2)

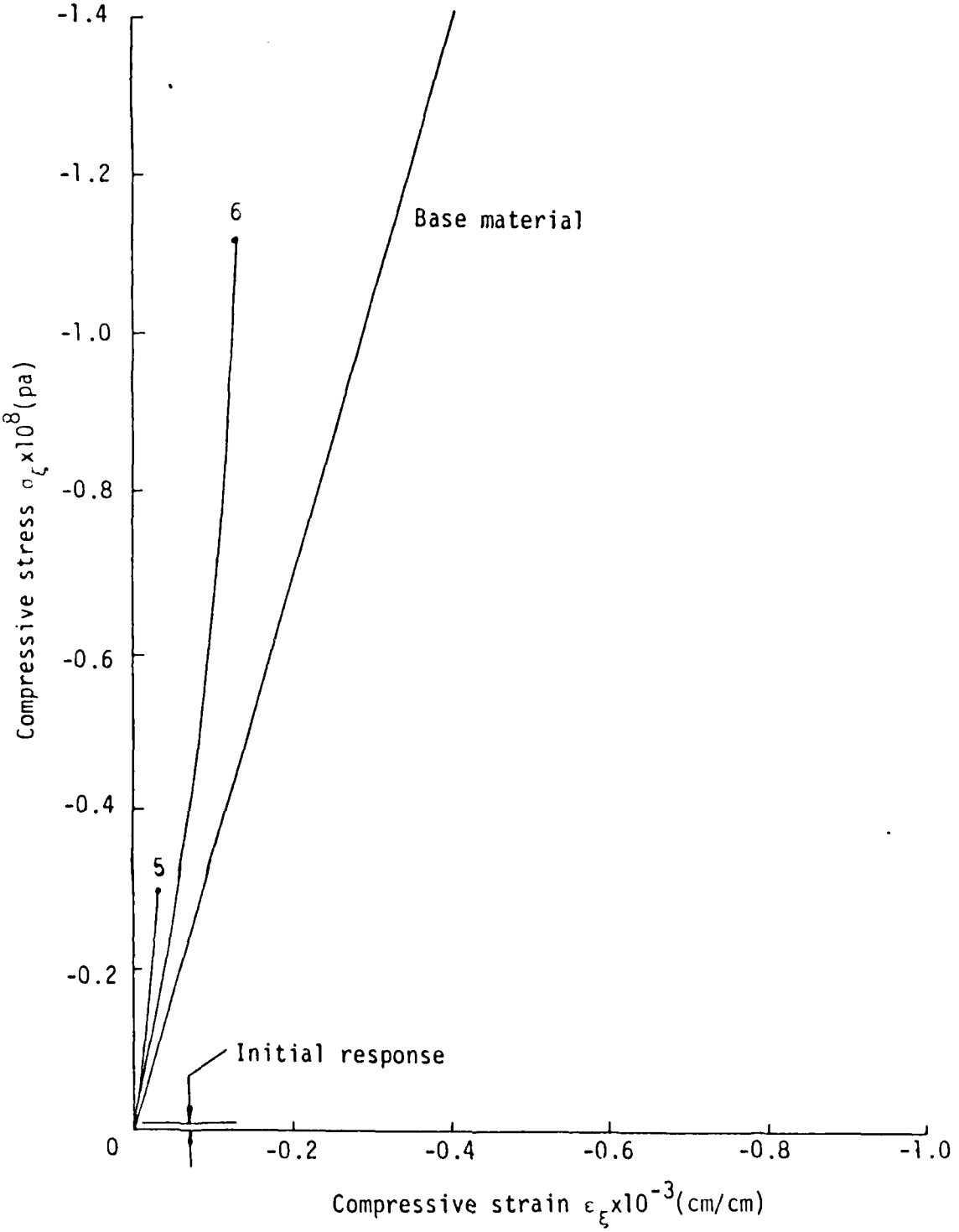

Figure 23. Local Stress And Strain Response At Point 5 And 6 In Projectile For t = 4 nsec And Quarter Scale (1:4)

only the initial response of tungsten or base material is used. The corner element in the projectile corresponding to point 6 in Figure 7(b) is stressed far beyond point 5 just inside the projectile. Both curves labelled 5 and 6 in Figures 21 to 23 are slightly nonlinear. This effect will become more obvious when damage begins to take place at the later stages. For details, reference can be made to Table 6 for the numerical values of σ_ξ and ε_ξ including those at t = 2 nsec. The dissipation energy density $\mathcal{D}$ as a function of time is given in Figures 24(a) to 24(c). In all cases, $\mathcal{D}$ increased slowly at first and then rises very quickly. This trend is particularly pronounced for point 6 even though the elapsed time is only 4 n sec. The

TABLE 6. Stress and Strain on Plane of Homogeneity at Point 5 and 6 in Projectile

	Point 6		Point 5	
Time t(nsec)	$\varepsilon_\xi \times 10^{-3}$ (cm/cm)	$\sigma_\xi \times 10^{8}$ (Pa)	$\varepsilon_\xi \times 10^{-3}$ (cm/cm)	$\sigma_\xi \times 10^{8}$ (Pa)
Full Scale (1:)				
2	-0.0762	-0.3981	-0.0198	-0.1141
4	-0.1635	-1.3548	-0.0387	-0.3653
Half Scale (1:2)				
2	-0.0677	-0.3557	-0.0176	-0.1019
4	-0.1454	-1.2168	-0.0344	-0.3280
Quarter Scale (1:4)				
2	-0.06097	-0.3230	-0.01585	-0.09256
4	-0.1309	-1.1159	-0.03097	-0.3007

dissipation at point 5 is relatively low as shown by the values in Table 7. Plotted in Figures 25(a) and 25(c) are the time histories of the temperature

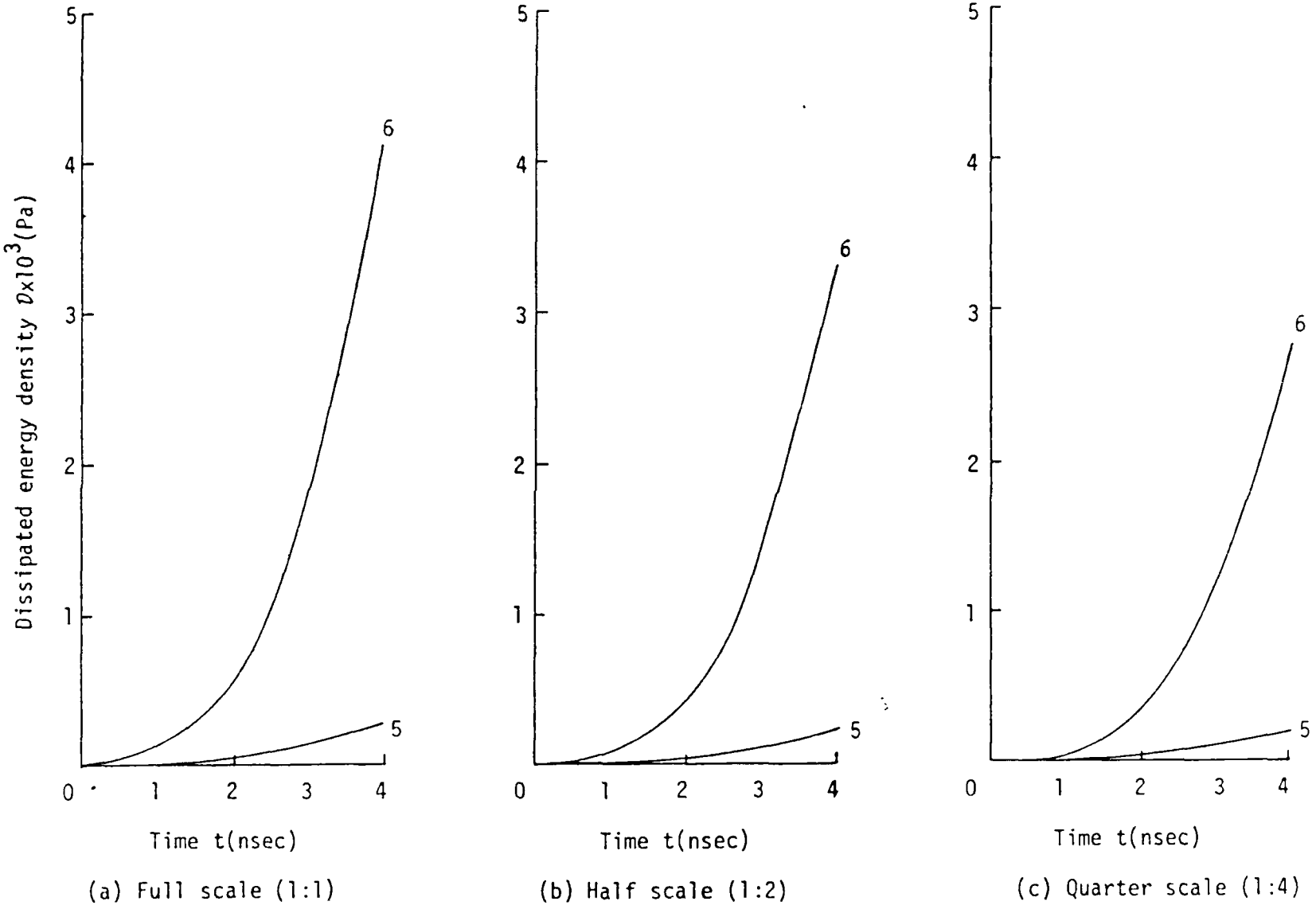

Figure 24. Time History Of Dissipated Energy Density At Point 5 And 6 In Tungsten Projectile

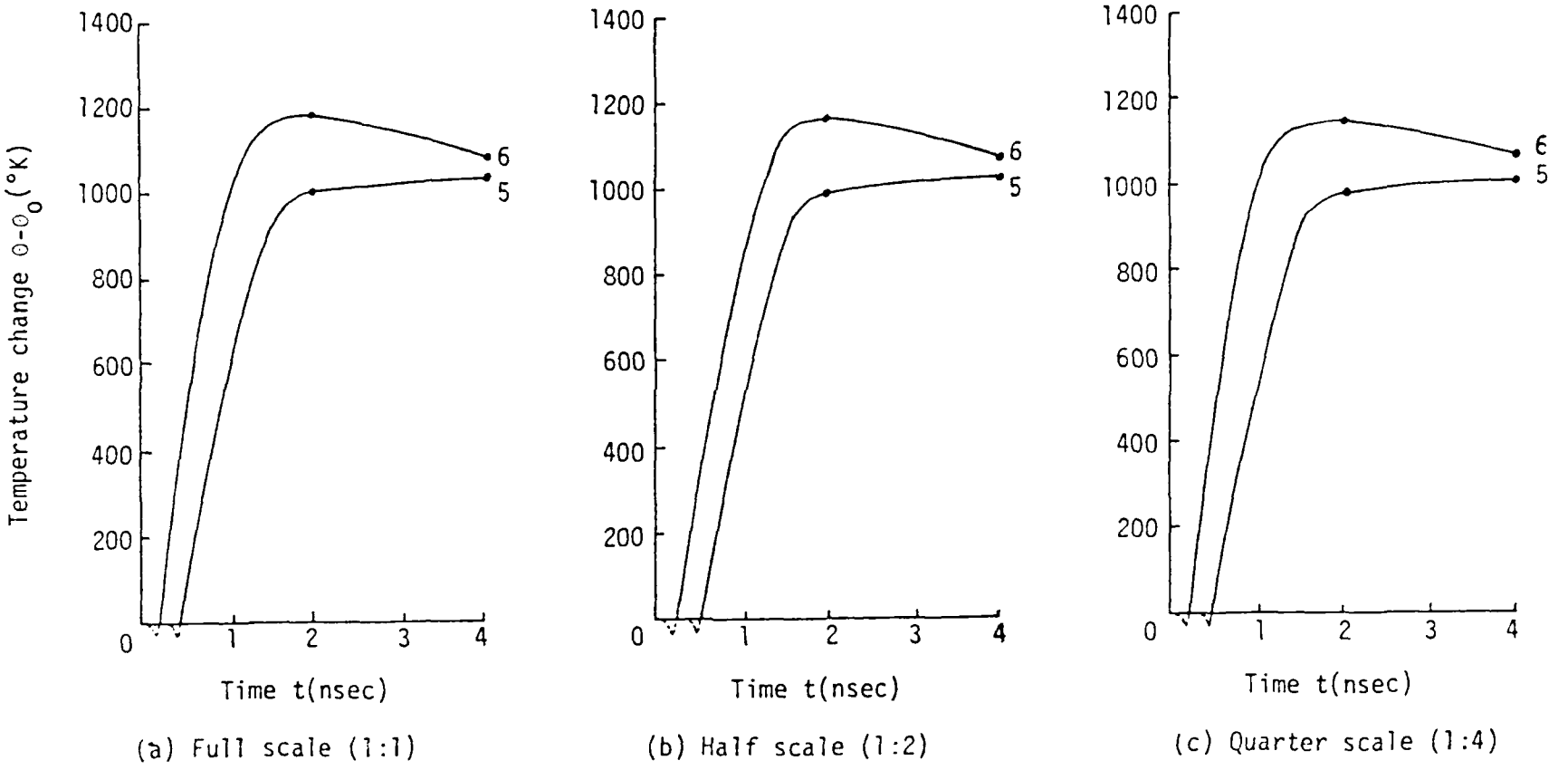

Figure 25. Time History Temperature Change At Point 5 and 6 In Tungsten Projectile With A Melting Temperature Of 3,683°K

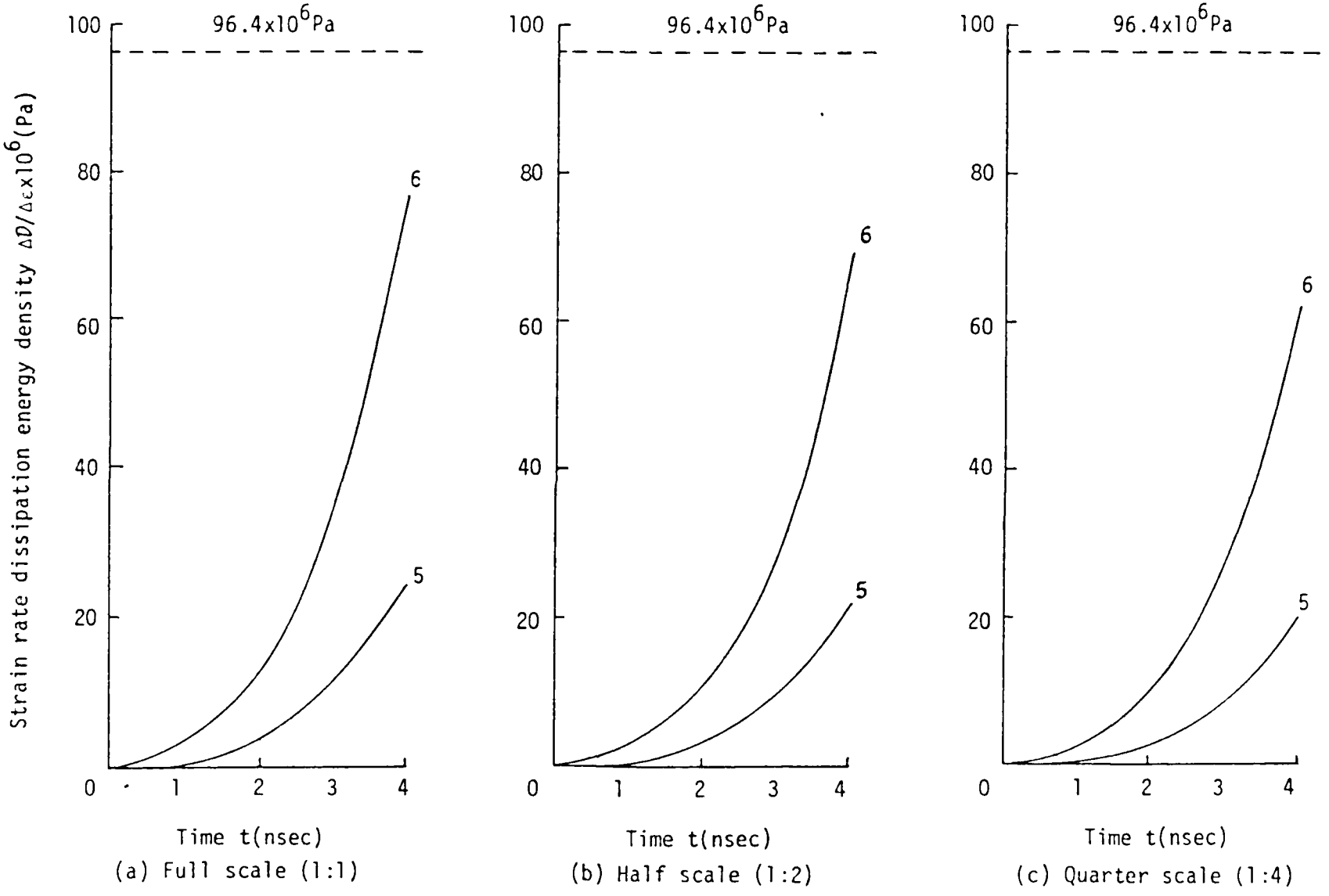

Figure 26. Time History Of Strain Rate Dissipation Energy Density At Point 5 And 6 In Tungsten Projectile

TABLE 7. Dissipation Energy Density and Strain Rate Dissipation Energy Density at Point 5 and 6 in Projectile

Time t(nsec)	Point 6 $\mathcal{D}\times10^3$ (Pa)	Point 6 $\Delta\mathcal{D}/\Delta\varepsilon\times10^6$ (Pa)	Point 5 $\mathcal{D}\times10^3$ (Pa)	Point 5 $\Delta\mathcal{D}/\Delta\varepsilon\times10^6$ (Pa)
Full Scale (1:1)				
2	0.5151	12.82	0.04532	3.27
4	4.0931	76.70	0.2756	24.43
Half Scale (1:2)				
2	0.4131	11.56	0.03625	3.30
4	3.2967	69.49	0.2216	22.32
Quarter Scale (1:4)				
2	0.3435	10.91	0.03003	3.10
4	2.7646	62.30	0.1855	20.68

change at points 5 and 6 in the projectile. A sign change in $\Theta-\Theta_0$ is again observed for small time. The temperature rose quickly in all the cases and then began to level off for t > 2 nsec. The plateaus of all the curves is substantially below the melting point of tungsten which occurs at 3,683°K as given in Table 1. Refer to Table 8 for numerical values of $\Theta-\Theta_0$. Finally, Figures 26(a) to 26(c) show the variations of $\Delta\mathcal{D}/\Delta\varepsilon$ with time. All the curves are below the threshold level of $\Delta Q/\Delta V = 96.4\times10^6$Pa for tungsten. No melting takes place in the projectile. Table 7 reveals that the highest $\Delta\mathcal{D}/\Delta\varepsilon$ value is 76.70×10^6Pa and this occurred at point 6 for t = 4 nsec.

TABLE 8. Temperature Change at Point 5 and 6 in Projectile

Time t(nsec)	Point 6 $\theta-\theta_o$ (°K)	Point 5 $\theta-\theta_o$ (°K)
Full Scale (1:1)		
2	1,181	1,000
4	1,085	1,028
Half Scale (1:2)		
2	1,169	992
4	1,076	1,021
Quarter Scale (1:4)		
2	1,149	979
4	1,059	1,007

4.4 Local Damage in Target

From the results in Sections 4.2 and 4.3 it can be concluded that only the target material next to the projectile corner is being damaged. The material in fact has locally undergone a phase transition where the solid has melted and turned into fluid. Such a behavior is reflected by the stress and strain curves in Figures 15 to 17. The shaded regions in Figures 27(a) to 27(c) are zones in which the solid has melted. Their volumes and areas denoted by V_m and A_m, respectively, are estimated and given in Table 9. The ratio V_m/A_m is the largest for the full scale system and the smallest for the quarter scale system. Their relative difference will change with time in a

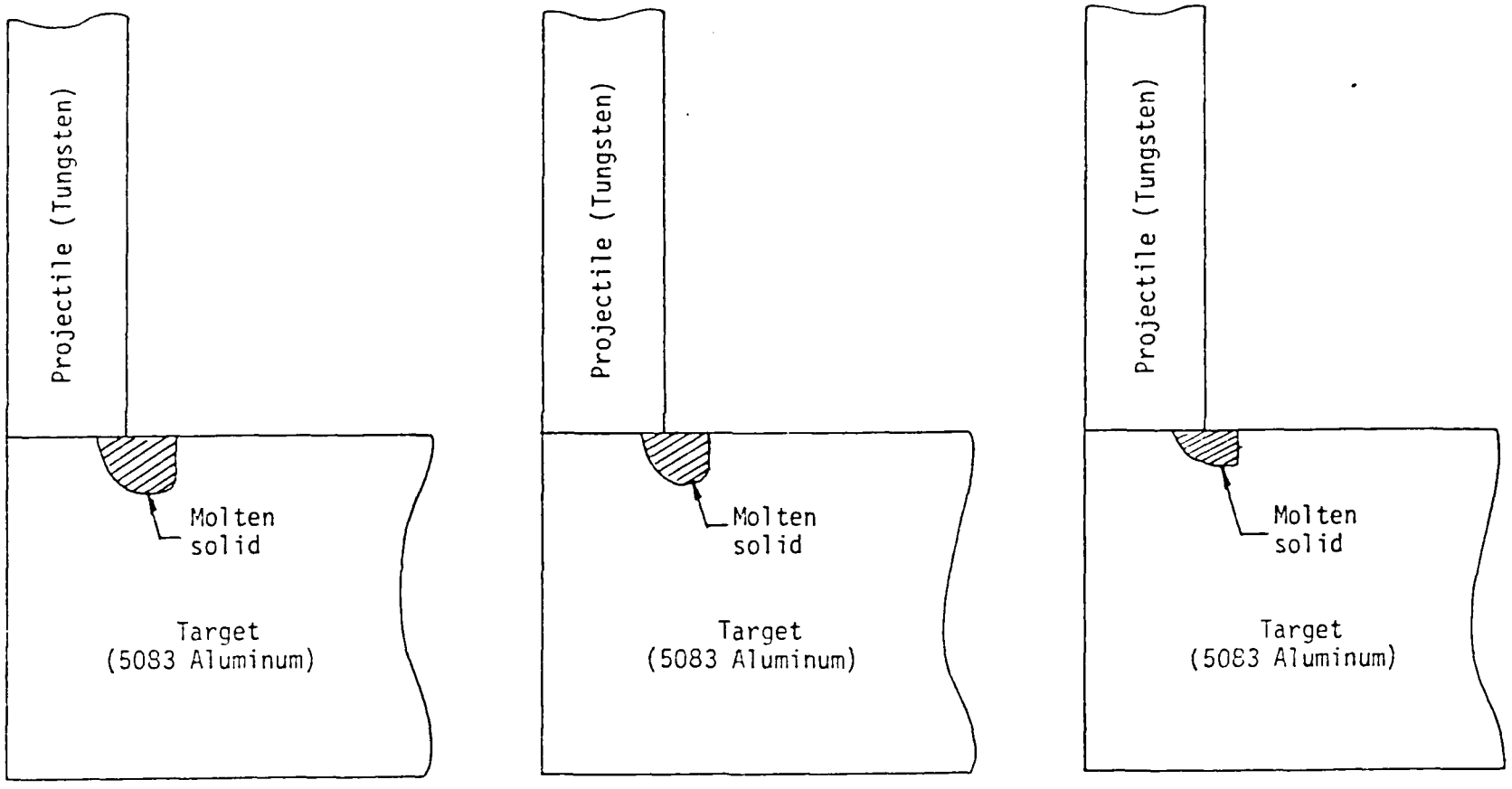

(a) Full scale (1:1)

(b) Half scale (1:2)

(c) Quarter scale (1:4)

Figure 27. Molten Local Region In Target/Projectile System For Time Different Scale Size At t = 4 msec

TABLE 9. Size of Melted Target Region at t = 4 nsec

Scale	Volume $V_m(cm^3)$	Area $A_m(cm^2)$	Ratio $V_m/A_m(cm)$	Impact Velocity m/sec
Full (1:1)	0.1325	0.9843	0.1346	9,000
Half (1:2)	0.0231	0.4528	0.0510	4,000
Quarter (1:4)	0.00391	0.1870	0.0209	1,000

nonlinear fashion. The complexities arising from the interaction of the geometric and kinematic parameters with damage have been clearly established. Any conclucions prior to a complete knowledge of the time damage process of the different scaled down systems would be premature.

V. ADDITIONAL REMARKS ON SCALING

The foregoing results provide sufficient evidence to the fact that damage caused by hypervelocity impact depends upon the complex interaction of several variables. There exists no simple laws of scaling. Geometric proportionality alone will not preserve the damage behavior of the projectile/target system. This can be demonstrated by solving the half scale problem with the projectile traveling at the same velocity as in the full scale case. Refer to the situations depicted in Figures 28(a) and 28(b). For the same projectile velocity of 9,000 m/sec or 30,000 ft/sec, it will be shown that the target damage in the half scale system will in no way resemble that of the full scale system at t = 4 nsec. This difference will increase with time.

Referring to the data in Table 10 and the sketches in Figures 28(a) and

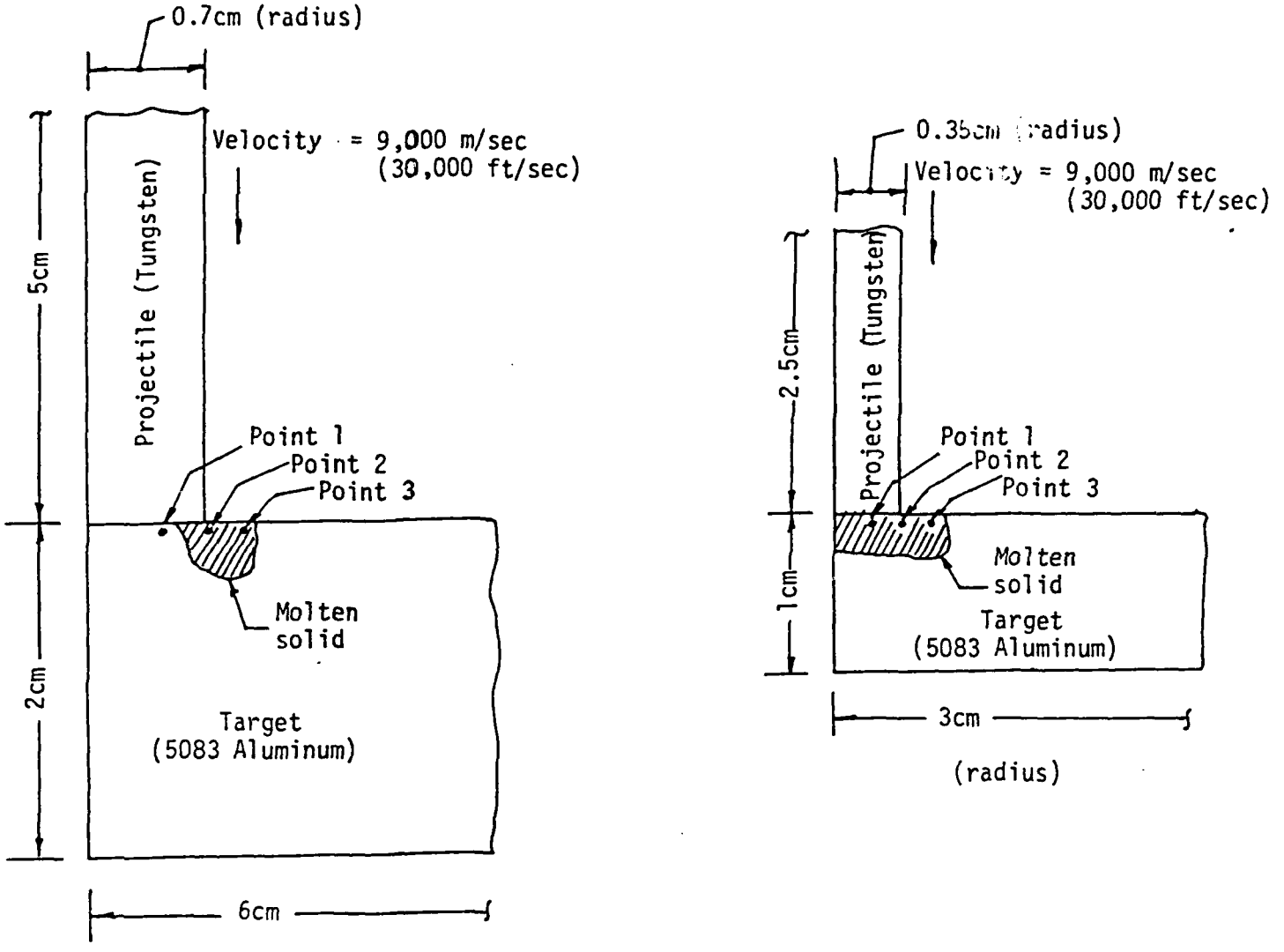

Figure 28. Cylindrical Projectile Impacting Circular Target Plate At Hypervelocity With Damage At t = 4 nsec

TABLE 10. Damage Zones for Full and Half Scale Projectile With the Same Initial Velocity of 9,000 m/sec and t = 4 nsec

Scale	Volume $V_m(cm^3)$	Area $A_m(cm^2)$	Ratio $V_m/A_m(cm)$
Full (1:1)	0.1325	0.9843	0.1346
Half (1:2)	0.1438	0.9940	0.1461

28(b), the damaged zone size for the scaled down model is larger than that of the full size model. The data in Table 11 also show that the elements at points 1, 2 and 3 in the half scale mode are all in the fluidic state while

TABLE 11. Dissipation Energy Density and Strain Rate Dissipation Energy Density at Point 1, 2 and 3 in Target for Half Scale System (1:2) with v_h = 9,000 m/sec

	Point 1		Point 2		Point 3	
Time t(nsec)	$\mathcal{D}x10^3$ (Pa)	$\Delta\mathcal{D}/\Delta\varepsilon x10^6$ (Pa)	$\mathcal{D}x10^3$ (Pa)	$\Delta\mathcal{D}/\Delta\varepsilon x10^6$ (Pa)	$\mathcal{D}x10^3$ (Pa)	$\Delta\mathcal{D}/\Delta\varepsilon x10^6$ (Pa)
2	0.6594	8.36	2.6342	12.20	1.3191	10.89
4	5.3501	40.67	18.7635	78.27	8.1179	68.96

point 1 remains unmelted in the full scale model where $\Delta\mathcal{D}/\Delta\varepsilon$ is below the critical value of $\Delta Q/\Delta V$ for tungsten. Moreover, the strain rate of energy dissipation in the half scale model is more intense. At point 3, a simple calculation shows that $(\Delta\mathcal{D}/\Delta\varepsilon)_{1:2}/(\Delta\mathcal{D}/\Delta\varepsilon)_{1:1}$ = 2.1 which is a factor two difference.

It is instructive to compare the normalized volume and surface area ratio of the damage zones for the full scale and half scale system

impacted at the same velocity. Making use of the dimensions specified and the data in Table 10, the following results are obtained:

$$\frac{(V_m/V_o)_{1:2}}{(V_m/V_o)_{1:1}} = 2.17 \quad ; \quad \frac{(A_m/A_o)_{1:2}}{(A_m/A_o)_{1:1}} = 2.02 \tag{29}$$

where V_o and A_o are the respective volume and area of the target. The normalized damage zone for the full scale and half scale differed by a factor of approximately two at t = 4 nsec. The difference will obviously alter with time.

The velocity of the projectile alone does not control the extent of target damage. In other words, the same degree of damage can be produced in a sub-scale model even though the projectile may be traveling at a much lower speed. Returning to the example discussed earlier in Section IV where the velocity of the half scale projectile was 4,000 m/sec rather than 9,000 m/sec. The damage zone at the same instance is more localized as shown in Figure 27(b). Making use of the data in Table 9, the normalized volume and area ratio of the full scale and half scale become

$$\frac{(V_m/V_o)_{1:2}}{(V_m/V_o)_{1:1}} = 0.348 \quad ; \quad \frac{(A_m/A_o)_{1:2}}{(A_m/A_o)_{1:1}} = 0.920 \tag{30}$$

Although the volume ratio is much less than unity, the surface one ratio is nearly one. The relative size of the damage area is being preserved at t = 4 nsec. Comparison of $(\Delta D/\Delta\varepsilon)_{1:2}$ and $(\Delta D/\Delta\varepsilon)_{1:1}$ can also be made for the element say again at point 3. From the data in Table 4, $(\Delta D/\Delta\varepsilon)_{1:2}/(\Delta D/\Delta\varepsilon)_{1:1} = 0.917$ at t = 4 nsec. The strain rate of dissipation is being preserved. Nearly the same ratio also prevails for points 1 and 2. Should

the damage be preserved for the entire time history, then the time variable must be normalized and scaled accordingly.

No useful information would be gained in scaling if the extremes of the geometric and kinematic parameters were chosen while emphasizing only the post mortem damage pattern or damage at any other specific time instance. Beyond certain combination of the projectile speed and target plate thickness, the resulting hole size in the target will be geometrically proportional to the projectile diameter. This represents the situation of overkill where the target no longer plays a sensitive role in the penetration process. In other words, most of the energy remains in the projectile as it passes through the target only a small portion of which is used to damage the material surrounding the hole. If this difference between the full scale and sub-scale system is to be neglected, then scaling is no longer the issue.

VI. REFERENCES

[1] G. C. Sih, "Mechanics and Physics of Energy Density Theory", J. of Theoretical and Applied Fracture Mechanics", Vol. 4, No. 3, pp 157-173, 1985.

[2] G. C. Sih and D. Y. Tzou, "Cooling and Heating of Uniaxial Tensile Coupon", Institute of Fracture and Solid Mechanics Technical Report, IFSM-85-137 Lehigh University, October, 1985.

[3] G. C. Sih, F. L. Lieu and C. K. Chao, "Thermal/Mechanical Damage of 6061-T6 Aluminum Tensile Specimen", Institute of Fracture and Solid Mechanics Technical Report IFSM-86-146, Lehigh University, October 1986.

[4] R. G. McQueen, S. P. Marsh, J. W. Taylor, J. N. Fritz and W. J. Carter, "Equations of State of Solids from Shock Wave Studies", in High Velocity Impact Phenomena edited by Ray Kinslow, pp. 293-417 Academic Press, New York, 1970.

[5] E. B. Royce, Implementation of GRAY, a Three-Phase Equation of State for Metals, Lawrence Livermore Laboratory, Dept. UCID-15871, 1971.

[6] M. I. Eskenazi, Fragment Shattering/Target Scaling Tests, Delco Systems Operations, Report R85-68, 1985.

[7] E. E. Gdoutos and G. C. Sih, "A Review of Material Behavior at High Strain Rates", Institute of Fracture and Solid Mechanics Technical Report IFSM-84-128, Lehigh University, October 1984.

[8] G. C. Sih and C. K. Chou, "Characteristics of Thermal/Mechanical Rate Effects for 6061-T6 Aluminum: Energy Density Theory", Institute of Fracture and Solid Mechanics Technical Report, IFSM-86-144, Lehigh University, September 1986.

DISTRIBUTION LIST

	No. of Copies
Office of Deputy Under Secretary of Defense for Research and Engineering (ET)	
ATTN: Mr. J. Persh, Staff Specialist for Materials and Structures (Room 3D1089)	1
The Pentagon	
Washington, DC 20301	
Commander	
U.S. Army Materiel Command	
ATTN: AMCLD, R. Vitali, Office of Laboratory Management	1
5001 Eisenhower Avenue	
Alexandria, VA 22333	
Director	
U.S. Army Strategic Defense Command	
ATTN: DASD-H-L, M. Capps	1
DASD-H-L, Dr. S. Proffitt	1
DASD-H-H, R. Buckelew	1
DASD-H-E, J. Katechis	1
P.O. Box 1500	
Huntsville, AL 35807	
Director	
U.S. Army Strategic Defense Command	
ATTN: DASD-H-Y, Col. K. Kawano	1
DASD-H-W, Dr. E. Wilkinson	1
DASD-H-W, J. Papadopoulos	1
DASD-H-W, S. Brockway	1
P.O. Box 1500	
Huntsville, AL 35807-3801	
Director	
Defense Nuclear Agency	
ATTN: SPAS, Maj. D. K. Apo	1
SPLH, J. W. Somers	1
SPLH, Dr. B. Steverding	1
Washington, DC 20305-1000	
Director	
Army Ballistic Research Laboratories	
ATTN: AMDAR-BLT, Dr. N. J. Huffington, Jr	1
AMDAR-BLT, Dr. T. W. Wright	1
Aberdeen Proving Ground, MD 21005	

	No. of Copies
Commander Air Force Materials Laboratory Air Force Systems Command ATTN: LNC, Dr. D. Schmidt Wright-Patterson Air Force Base Dayton, OH 45433	1
Commander BMO/ABRES Office ATTN: Capt. S. Opel Norton Air Force Base, CA 92409	1
Commander Air Force Materials Laboratory ATTN: AFML/MBM, Dr. S. W. Tsai Wright-Patterson Air Force Base Dayton, OH 45433	1
Commander Naval Ordinance Systems Command ATTN: ORD-03331, Mr. M. Kinna Washington, DC 20360	1
Naval Postgraduate School ATTN: Code NC4(67WT), Prof. E. M. Wu Monterey, CA 93943	1
Commander Naval Surface Weapons Center ATTN: C. Lyons C. Rowe Silver Springs, MD 20910	1 1
Defense Documentation Center Cameron Station, Bldg. 5 5010 Duke Station Alexandria, VA 22314	2
Aerospace Corporation ATTN: Dr. R. Cooper P.O. Box 92957 Los Angeles, CA 90009	1
AVCO Corporation Government Products Group ATTN: Dr. W. Reinecke P. Rolincik 201 Lowell Street Wilmington, MA 01997	1 1

	No. of Copies
ETA Corporation ATTN: D. L. Mykkinen P.O. Box 6625 Orange, CA 92667	1
Fiber Materials, Inc. ATTN: M. Subilia, Jr. L. Landers R. Burns Biddeford Industrial Park Biddeford, ME 04005	1 1 1
General Electric Company Advanced Materials Development Laboratory ATTN: K. Hall J. Brazel 3198 Chestnut Street Philadelphia, PA 19101	1 1
General Dynamics Corporation Convair Division ATTN: J. Hertz 5001 Kearny Villa Road San Diego, CA 92138	1
General Research Corporation ATTN: Dr. R. Wengler Dr. R. Parisse J. Green 5383 Hollister Avenue Santa Barbara, CA 93111	1 1 1
Hercules Aerospace Corporation ATTN: Dr. S. W. Beckwith (X2F5) P.O. Box 98 Magna, UT 84044-0098	1
Kaman Sciences Corporation ATTN: Dr. D. C. Williams P.O. Box 7463 Colorado Springs, CO 80933	1
Ktech ATTN: Dr. D. Keller 911 Pennsylvania Avenue, N.E. Albuquerque, NM 87110	1
Lawrence Livermore National Laboratory ATTN: Dr. W. W. Feng P.O. Box 808 (L-342) Livermore, CA 94550	1

	No. of Copies
Lehigh University Institute of Fracture and Solid Mechanics ATTN: Dr. George C. Sih Packard Lab, Bldg. 39 Bethlehem, PA 18015	1
Los Alamos National Laboratory ATTN: Dr. W. D. Birchler, Mail Stop G787 Henry L. Horak Los Alamos, NM 87545	1 1
Martin Marietta Aerospace ATTN: V. Hewitt Frank H. Koo P.O. Box 5837 Orlando, FL 32805	1 1
Massachusetts Institute of Technology Department of Aeronautics and Astronautics ATTN: Prof. T. H. H. Pian (Room 311, Bldg. 73) Cambridge, MA 02139	1
Pacifica Technology, Inc. ATTN: Dr. Ponsford P.O. Box 148 Del Mar, CA 92014	1
Radkowski Associates ATTN: Dr. P. Radkowski P.O. Box 5474 Riverside, CA 92507	1
Rohr Industries, Inc. ATTN: Dr. T. H. Tsiang MZ-19T P.O. Box 878 Chula Vista, CA 92012-0878	1
Sandia Laboratories ATTN: Dr. W. Alzheimer Dr. M. Forrestal Dr. E. P. Chen, Div. 1524 P.O. Box 5800 Albuquerque, NM 87115	1 1 1
Southwest Research Institute ATTN: A. Wenzel 8500 Culebra Road San Antonio, TX 78206	1
SPARTA, Inc. ATTN: J. Wonacott J. Glatz 1055 Wall Street Suite 200 P.O. Box 1354 La Jolla, CA 92038	1 1

	No. of Copies
Terra Tek, Inc. ATTN: Dr. A. H. Jones 420 Wakara Way Salt Lake City, UT 84108	1
University of Washington ATTN: K. Y. Lin FS-10, Guggenhein Bldg. Seattle, WA 98195	1
Commander U.S. Army Laboratory Command ATTN: SLCIS-IM-TL 2800 Powder Mill Road Adelphi, MD 20783-1145	1
Commander Defense Technical Information Center ATTN: DTIC-FDAC Cameron Station, Building 5, 5010 Duke Street Alexandria, VA 22304-6145	2
Director U.S. Army Materials Technology Laboratory ATTN: SLCMT-IML	2
SLCMT-IMA-P	1
SLCMT-ISC	1
SLCMT-BM,J. F. Dignam	1
SLCMT-BM, S. C. Chou	25
SLCMT-BM, L. R. Aronin	1
SLCMT-BM, D. P. Dandekar	1
Watertown, MA 02172-0001	

U.S. Army Materials Technology Laboratory
Watertown, Massachusetts 02172-0001
SUB-SCALING OF PROJECTILE/TARGET SYSTEM
DAMAGED BY HYPERVELOCITY
G. C. Sih
Comptek Corporation
Allentown, PA 18103
Final Report MTL TR 87-17, March 1987
54 pp-illus-tables, Contract DAAG46-85-C-0061
AMCMS Code: 69200R897 A050
Final Report, 8/28/85 through 9/30/86

AD ________
UNCLASSIFIED
UNLIMITED DISTRIBUTION

Key Words

Hypervelocity impact
Scale models
Damage
Fracture
Finite element
Strain energy methods
Numerical analysis
Phase transformation

Preliminary efforts are made to develop a methology for analyzing the progressive failure of projectile/target systems under hypervelocity impact. Particular emphasis is placed on the thermal/mechanical interaction effects not only for evaluating the change in the local strain rates and material properties but also in finding the temperature and latent heat at which the solid may locally transform into liquid and/or gas. Such a transition can be accurately determined by the inflection points on the time dependent H-function curve that serves as a measure of the order and/or disorder of a physical system.

Damage of a tungsten projectile with a 1:3.57 aspect ratio impacting a 5083 aluminum target with a 1:3 aspect ratio at 9,000 m/sec is evaluated. Melting of the target material is predicted in the region directly underneath the projectile corner. Geometrically and metallurgically similar systems scaled down one-half and one-quarter in size are also considered resulting in damage zones that are not proportional. Such information is useful for developing scaling relations even though the results are nonlinear functions of the governing parameters.

U.S. Army Materials Technology Laboratory
Watertown, Massachusetts 02172-0001
SUB-SCALING OF PROJECTILE/TARGET SYSTEM
DAMAGED BY HYPERVELOCITY
G. C. Sih
Comptek Corporation
Allentown, PA 18103
Final Report MTL TR 87-17, March 1987
54 pp-illus-tables, Contract DAAG46-85-C-0061
AMCMS Code: 69200R897 A050
Final Report, 8/28/85 through 9/30/86

AD ________
UNCLASSIFIED
UNLIMITED DISTRIBUTION

Key Words

Hypervelocity impact
Scale models
Damage
Fracture
Finite element
Strain energy methods
Numerical analysis
Phase transformation

Preliminary efforts are made to develop a methology for analyzing the progressive failure of projectile/target systems under hypervelocity impact. Particular emphasis is placed on the thermal/mechanical interaction effects not only for evaluating the change in the local strain rates and material properties but also in finding the temperature and latent heat at which the solid may locally transform into liquid and/or gas. Such a transition can be accurately determined by the inflection points on the time dependent H-function curve that serves as a measure of the order and/or disorder of a physical system.

Damage of a tungsten projectile with a 1:3.57 aspect ratio impacting a 5083 aluminum target with a 1:3 aspect ratio at 9,000 m/sec is evaluated. Melting of the target material is predicted in the region directly underneath the projectile corner. Geometrically and metallurgically similar systems scaled down one-half and one-quarter in size are also considered resulting in damage zones that are not proportional. Such information is useful for developing scaling relations even though the results are nonlinear functions of the governing parameters.

U.S. Army Materials Technology Laboratory
Watertown, Massachusetts 02172-0001
SUB-SCALING OF PROJECTILE/TARGET SYSTEM
DAMAGED BY HYPERVELOCITY
G. C. Sih
Comptek Corporation
Allentown, PA 18103
Final Report MTL TR 87-17, March 1987
54 pp-illus-tables, Contract DAAG46-85-C-0061
AMCMS Code: 69200R897 A050
Final Report, 8/28/85 through 9/30/86

AD ________
UNCLASSIFIED
UNLIMITED DISTRIBUTION

Key Words

Hypervelocity impact
Scale models
Damage
Fracture
Finite element
Strain energy methods
Numerical analysis
Phase transformation

Preliminary efforts are made to develop a methology for analyzing the progressive failure of projectile/target systems under hypervelocity impact. Particular emphasis is placed on the thermal/mechanical interaction effects not only for evaluating the change in the local strain rates and material properties but also in finding the temperature and latent heat at which the solid may locally transform into liquid and/or gas. Such a transition can be accurately determined by the inflection points on the time dependent H-function curve that serves as a measure of the order and/or disorder of a physical system.

Damage of a tungsten projectile with a 1:3.57 aspect ratio impacting a 5083 aluminum target with a 1:3 aspect ratio at 9,000 m/sec is evaluated. Melting of the target material is predicted in the region directly underneath the projectile corner. Geometrically and metallurgically similar systems scaled down one-half and one-quarter in size are also considered resulting in damage zones that are not proportional. Such information is useful for developing scaling relations even though the results are nonlinear functions of the governing parameters.

U.S. Army Materials Technology Laboratory
Watertown, Massachusetts 02172-0001
SUB-SCALING OF PROJECTILE/TARGET SYSTEM
DAMAGED BY HYPERVELOCITY
G. C. Sih
Comptek Corporation
Allentown, PA 18103
Final Report MTL TR 87-17, March 1987
54 pp-illus-tables, Contract DAAG46-85-C-0061
AMCMS Code: 69200R897 A050
Final Report, 8/28/85 through 9/30/86

AD ________
UNCLASSIFIED
UNLIMITED DISTRIBUTION

Key Words

Hypervelocity impact
Scale models
Damage
Fracture
Finite element
Strain energy methods
Numerical analysis
Phase transformation

Preliminary efforts are made to develop a methology for analyzing the progressive failure of projectile/target systems under hypervelocity impact. Particular emphasis is placed on the thermal/mechanical interaction effects not only for evaluating the change in the local strain rates and material properties but also in finding the temperature and latent heat at which the solid may locally transform into liquid and/or gas. Such a transition can be accurately determined by the inflection points on the time dependent H-function curve that serves as a measure of the order and/or disorder of a physical system.

Damage of a tungsten projectile with a 1:3.57 aspect ratio impacting a 5083 aluminum target with a 1:3 aspect ratio at 9,000 m/sec is evaluated. Melting of the target material is predicted in the region directly underneath the projectile corner. Geometrically and metallurgically similar systems scaled down one-half and one-quarter in size are also considered resulting in damage zones that are not proportional. Such information is useful for developing scaling relations even though the results are nonlinear functions of the governing parameters.

END

FILMED

MARCH, 1988

DTIC